J. Fluid Mech. (1991), *vol.* 232, *pp.* 99–131
Printed in Great Britain

Vortex-induced boundary-layer separation. Part 1. The unsteady limit problem $Re \to \infty$

By VALLORIE J. PERIDIER,[1] F. T. SMITH[2] AND J. D. A. WALKER[3]

[1] Department of Mechanical Engineering, Temple University, Philadelphia, PA 19122, USA
[2] Department of Mathematics, University College London, Gower Street, London WC1E 6BT, UK
[3] Department of Mechanical Engineering and Mechanics, Lehigh University, Bethlehem, PA 18015, USA

(Received 28 September 1990 and in revised form 23 April 1991)

The unsteady boundary-layer flow produced by a two-dimensional vortex in motion above an infinite plane wall in an otherwise stagnant fluid is considered in the limit of infinite Reynolds number. This study is part of a continuing investigation into the nature of the physical processes that occur near the surface in transitional and fully turbulent boundary layers. The adverse pressure gradient due to the vortex leads to the development of a zone of recirculation in the viscous flow near the surface, and the boundary-layer flow then focuses rapidly toward an eruption along a band which is very narrow in the streamwise direction. The evolution of the unsteady boundary layer is posed in Lagrangian coordinates and computed using an efficient, factored ADI numerical method. The boundary-layer solution is found to develop a separation singularity and to evolve toward a terminal stage which is generic in two-dimensional unsteady flows. The computed results are compared with the results of asymptotic theory of two-dimensional boundary-layer separation and the agreement is found to be excellent.

1. Introduction

Unsteady boundary-layer separation occurs in a number of important applications such as the flows encountered in turbomachinery and on pitching airfoil surfaces (McCroskey 1982; Smith 1982; Elliott & Smith 1987, and the references therein); in addition, in turbulent flows near walls, it is well known (as discussed subsequently) that the wall-layer flow breaks down intermittently and develops strong localized eruptions (Walker *et al.* 1989; Smith *et al.* 1991). At high Reynolds number, Re, the separation process is invariably initiated in a thin unsteady viscous boundary layer near a solid surface in the form of the evolution of a closed recirculating eddy, in a region where the mainstream pressure gradient is adverse. In the classical studies of impulsive motion past bluff bodies (see, for example, Collins & Dennis 1973; Riley 1975), the recirculation zone is generally attached to the body and the first appearance of reversed flow was traditionally referred to as separation (Riley 1975). For impulsively started flow past a bluff body, the vanishing of the wall shear generally signals the onset of reversed flow within the boundary layer. The impulsively started circular cylinder has been studied extensively (see, for example, Collins & Dennis 1973; Van Dommelen 1981), and at the initiation of the motion, the wall shear is positive everywhere. Shortly thereafter the wall shear vanishes at the

rear stagnation point and a point of zero wall shear moves rapidly upstream along the cylinder surface. At any time, the point of zero shear defines the upstream location of a growing region of recirculating flow (and negative wall shear) which is attached to the back portion of the cylinder. At this stage of development, the entire flow field may be still viewed as double-structured, consisting of an outer inviscid flow and a (as yet) thin viscous boundary layer immediately adjacent to the surface. Eventually, the thickening boundary layer must grow to the point where the boundary-layer thickness is comparable with the dimensions of the cylinder and the external flow is thereby significantly affected. Such an event will be referred to here as an unsteady viscous–inviscid interaction, and since such interactions occur in a variety of situations, it is important to understand why they initiate and how they develop in time. Riley (1975) has used the term 'breakaway' to describe the first breakdown of the boundary-layer assumption, namely that the boundary layer is thin. On the basis of a similarity solution due to Proudman & Johnson (1962) which predicts exponential thickening of the boundary layer at the rear stagnation point, Riley (1975) argued that the onset of interaction with the external flow possibly occurs only at infinite time on the boundary-layer timescale and in the process the external flow is simply displaced from the cylinder surface. The correct nature of the interaction is considerably more complicated and localized in nature than this and was eventually elucidated by Van Dommelen & Shen (1980), whose work will be discussed subsequently.

For impulsive motion past stationary bluff bodies, the current streamwise location (as well as the first appearance) of a point of zero wall shear is an important defining feature of the instantaneous flow structure. However, unsteady boundary-layer flows involve a rich variety of complex phenomena and the subject of laminar unsteady separation has been controversial over the past twenty years. Two main points have been at issue, namely: (i) how unsteady separation should be defined, and (ii) whether or not a singularity evolves at finite time within the solution of the boundary-layer equations in all cases of unsteady separation (see, for example, Riley 1975; Williams 1977 and Cousteix 1986). Sears & Telionis (1971, 1975) pointed out that the traditional criterion of vanishing of the wall shear and the onset of reversed flow are not sufficiently general to describe all cases of unsteady separation; they quote examples involving moving walls where vanishing of the wall shear is not a significant feature of the flow structure nor a precursor to the interaction eventually taking place. More complex examples are described by Walker (1978) and Ece, Walker & Doligalski (1984). The model problem of interest in the present study was originally considered by Walker (1978) and corresponds to the boundary layer induced by a vortex in motion above an infinite plane wall in an otherwise stagnant fluid, as indicated in figure 1. In a frame of reference moving with the vortex, there is flow in the boundary layer in both the upstream and downstream directions even in the early stages of the motion (Walker 1978), and the conventional notions of 'reversed flow' do not apply. As time passes, a recirculating eddy forms and starts to grow within the boundary layer, but the eddy is aloft and not attached to the wall. This first appearance of closed instantaneous streamlines is one possible definition of separation which is in the spirit of the classical view of separation for flow past fixed walls. The evolution of a recirculating region is normally followed by dramatic growth of the eddy and it is also usually a precursor to a strong interaction with the mainstream (see also Ersoy & Walker 1985, 1986), or in other words 'breakaway'. Another relevant example is the impulsively started translating and rotating circular cylinder considered by Ece *et al.* (1984). Here closed recirculating eddies appear

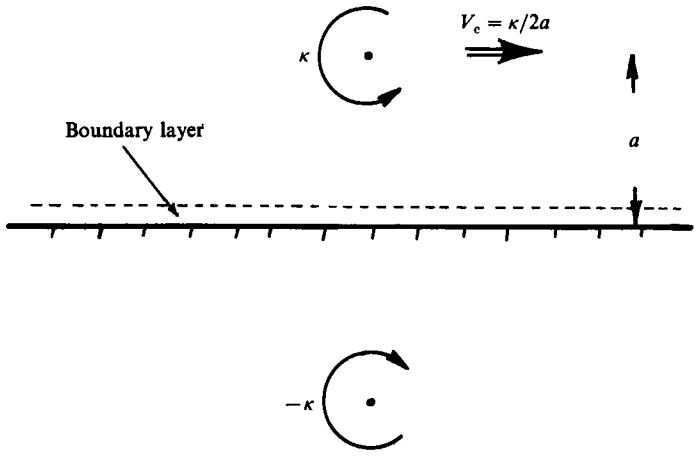

FIGURE 1. Schematic diagram of the geometry for the model problem with image vortex below the wall.

within the boundary layer shortly after the impulsive start. Again, however, these eddies are not attached to the wall, and their birth is not associated with a zero in the wall shear.

An alternative and rather different view of boundary-layer separation was proposed by Sears & Telionis (1971, 1975) in order to generalize the definition of separation. They argued that separation should be defined in all cases as that instant when a singularity develops in the boundary-layer solution. It is useful here to discuss the physical implications of the evolution of a singularity. The boundary-layer equations are an exact subset of the Navier–Stokes equations in the limit as $Re \to \infty$ and describe an attached flow in a thin layer near the surface. The boundary-layer solution is described in part by the scaled variables

$$y = Re^{\frac{1}{2}} Y, \quad v = Re^{\frac{1}{2}} V, \tag{1}$$

where Y measures distance normal to the surface and V is the corresponding velocity component. As long as the boundary layer is thin and attached, y and v are $O(1)$. On the other hand, when rapid thickening occurs and the fluid particles are eventually located at a distance greater than $O(Re^{-\frac{1}{2}})$ from the wall, y must become large in order to overcome the infinite limiting value of Re. Similarly with the evolution of large updraughts having a magnitude greater than $O(Re^{-\frac{1}{2}})$, v must become singular. Consequently, the definition of separation in this context is similar to what Riley (1975) has termed 'breakaway' and some other authors (Williams 1977) have termed breakdown. The formation of a singularity may be thought of as the first time at which an erupting boundary layer has a significant effect on the external inviscid flow; put another way, it represents the onset of viscous–inviscid interaction between the boundary layer and the outer mainstream flow, for which new scalings of the Navier–Stokes equations are required to describe the flow problem locally.

Sears & Telionis (1971, 1975) put forth what is now known as the MRS model of separation (after Moore 1958, Rott 1956 and Sears) in which they envisaged a moving stagnation point termed the 'centre of separation' (which in general is above the wall), with a singularity forming somewhere on the zero vorticity line at finite time. Note that such a line is present whenever regions of recirculating flow develop in the boundary layer. Sears & Telionis (1971) also argued that the singularity

defining 'separation' was similar to the Goldstein (1948) singularity, which is known to occur in steady two-dimensional boundary-layer solutions when the mainstream pressure gradient is adverse and prescribed. The conjectures of Sears & Telionis (1971) were controversial, particularly the proposed Goldstein singularity structure (Riley 1975; Williams 1977). A large number of attempts were made to verify the proposed behaviour through numerical calculations, some of which are discussed by Williams (1977). By and large, these numerical studies were inconclusive and were hampered by two problems. First, as Williams (1977) has noted, the speed at which the 'centre of separation' moves is unknown in any given problem; thus the conjectured streamline pattern near the 'centre of separation' (Sears & Telionis 1971) can only be clearly observed in a moving reference frame whose velocity is unknown *a priori*. Second, all boundary-layer integrations prior to 1980 were carried out using a mesh fixed in space and the conventional Eulerian description of the fluid motion. Although it was evident that severe numerical difficulties were being encountered (Collins & Dennis 1973; Walker 1978; Cebeci 1986) in such integrations, it was not possible to definitively pinpoint the reasons for the failures. In most situations, the boundary-layer solutions were observed to start to develop relatively large normal velocities in a local zone which was narrow in the streamwise direction. Furthermore, despite a variety of attempts to pack grid points into the zone (see, for example, Cebeci 1986), it was not possible to continue the integrations with good accuracy and thereby to reach the anticipated singular structure.

A significant advance was made by Van Dommelen & Shen (1980) who pointed out that Lagrangian variables are ideally suited to the computation of unsteady boundary-layer flows that develop an eruptive character. In a conventional Eulerian formulation, the changes in velocities (u, v) are computed at a large number of fixed mesh points in the (x, y)-space as the flow evolves. The Lagrangian viewpoint is fundamentally different, wherein the velocities of a large number of fluid particles are identified at points on a spatial grid at some initial time; the subsequent velocity and position of each fluid particle is then calculated as a function of time (and the initial starting location in the grid). A principal advantage of Lagrangian variables for the boundary-layer equations is that the streamwise momentum equation involves only the streamwise particle positions x and velocity u and not the normal coordinate y and velocity v. It is y and v which become large and eventually singular as a boundary layer evolves toward an eruption; at the same time, the computed quantities x and u both remain regular.

Van Dommelen & Shen (1980, 1982) performed a numerical integration of the boundary layer on an impulsively started circular cylinder. For the first time, the terminal boundary-layer state was reached via an accurate numerical integration and the nature of the developing interaction with the outer flow was revealed. In the latter stages of the calculation, the boundary-layer flow focused into a band which was narrow in the streamwise direction and which forms on the upstream side of the recirculation zone. In the terminal state, the displacement thickness evolves toward a sharp spike which is infinitely long on the boundary-layer scale; on the scale of the outer external flow, the 'spike' appears as a small sharp eruption at a point. Van Dommelen & Shen (1982) and Elliott, Cowley & Smith (1983) have obtained analytical solutions for the possible forms of the terminal singularity structure for two-dimensional unsteady boundary layers. The 'spike' that developed in the displacement surface in the calculations of Van Dommelen & Shen (1980) was found to have a complex unsteady structure. As the boundary layer erupts, it bifurcates into three tiers consisting of: (i) a layer of $O(1)$ y-thickness near the surface; (ii) a

layer of $O(1)$ y-thickness which moves rapidly away from the surface and forms the sides of the erupting spike; and (iii) an intermediate vorticity-depleted zone which thickens like $(t_s-t)^{-\frac{1}{2}}$ as t approaches the eruption time t_s. The dynamics of the eruptive process is driven by the intermediate zone, within which the velocity is almost uniform. The theory of Elliott *et al.* (1983) suggests that this terminal boundary-layer structure, wherein the flow rapidly focuses into a narrow spike, may be a generic state reached by most unsteady two-dimensional erupting boundary layers. As the eruptive state is approached the boundary-layer solution becomes independent, to leading order, of the adverse pressure gradient in the mainstream flow which originally initiated the process. The onset of 'spike-like' behaviour in displacement thickness had been observed in a variety of different circumstances, including the boundary layer induced by: (i) a vortex convected in a uniform flow (Doligalski & Walker 1984; Chuang & Conlisk 1989; Conlisk 1989), (ii) counter-rotating vortex pairs (Ersoy & Walker 1985, 1986), and (iii) vortex rings moving toward a surface (Walker *et al.* 1987). However, the latter computations were all carried out using an Eulerian formulation and it was generally not possible to continue the integrations all the way to the eruptive state (one exception is the series approach described by Cowley 1983). At present, Van Dommelen's (1981) calculations for the circular cylinder appear to be the only ones to reach the terminal state described by Elliott *et al.* (1983).

In the present study, a physical situation rather different from the impulsively started cylinder is considered, namely the unsteady boundary layer induced by a vortex above an infinite plane wall in an otherwise stagnant fluid. The motion is impulsively started from rest (Walker 1978) and the numerical solutions described herein were obtained in Lagrangian coordinates. Although the Lagrangian equations bear some similarity to the momentum equations in the Eulerian frame, it was found that conventional algorithms, to advance the solution forward in time, did not work well. Therefore an upwind-downwind alternating-direct-implicit (ADI) method was developed in this study. It is shown here that the boundary-layer solution ultimately evolves toward a sharply focused eruption and to a terminal state virtually identical to that described by Elliott *et al.* (1983).

The vortex-induced separation problem is also of physical interest in relation to the regenerative processes that take place in turbulent boundary layers and in flows undergoing transition to turbulence. For a fully developed turbulent boundary layer, the convected hairpin vortex (Head & Bandyopadhyay 1981; Acarlar & Smith 1987*a*, *b*; Walker *et al.* 1989; Smith *et al.* 1990, 1991; Walker 1990*a*, *b*) appears to be the dominant flow structure. As this vortex moves near the wall it is able to provoke a discrete eruption of the viscous flow below in an event usually known as bursting (Smith *et al.* 1990, 1991; Walker 1990*b*). Similar phenomena also occur in transition. The situation considered in this paper is the simplest case of a vortex-induced eruption and a number of experiments (Harvey & Perry 1971; Chu & Falco 1988; Walker *et al.* 1987) have clearly shown the general features of the subsequent interaction. In a turbulent boundary layer, the eruptive activity is three-dimensional in which the boundary layer erupts along a crescent-shaped ridge (Smith *et al.* 1990, 1991; Walker 1990*b*; Van Dommelen & Cowley 1990); however, the process may be viewed as quasi-two-dimensional in the sense that in a plane normal to the ridge, the eruption is similar to the two-dimensional situation. Consequently the model problem considered in this study seems representative of the physical processes that take place in more complex environments and also is illustrative of the numerical difficulties inherent in computing an erupting boundary layer.

2. Formulation

Consider a rectilinear vortex of strength κ which is located in an otherwise stagnant fluid above an infinite plane wall; at $t = 0$ the vortex is located at a distance a above the wall as indicated in figure 1. Inviscid theory (Walker 1978) predicts that a vortex of positive rotation (as shown in figure 1) is convected in the velocity field of its image, consequently moving to the right with constant velocity given by

$$V_c = \kappa/2a, \tag{2}$$

and remaining at constant height, a, above the wall. The inviscid solution is not uniformly valid, however, and a thin unsteady boundary layer develops along the wall in order to satisfy the no-slip condition. The boundary layer has a thickness $O(Re^{-\frac{1}{2}})$, where the Reynolds number may be defined by

$$Re = aV_c/\nu, \tag{3}$$

and ν is the kinematic viscosity. Dimensionless variables are defined in terms of the length a, the self-convection speed V_c, and the timescale (a/V_c). Furthermore, since the boundary layer develops in response to the moving vortex, it is convenient to transform to a frame of reference which moves uniformly with the vortex. In this frame, the wall moves to the left with velocity -1, and the mainstream velocity induced at the boundary-layer edge is steady and given by (Walker 1978)

$$U_\infty(x) = -1 + U_e(x), \quad U_e(x) = \frac{4}{x^2+1}. \tag{4}$$

Here x measures streamwise distance in the convected frame relative to the location at the vortex core at $x = 0$.

For the boundary-layer flow, a scaled normal velocity v and coordinate y are defined in terms of the corresponding physical quantities V and Y by (1). In the conventional Eulerian formulation, the two-dimensional boundary-layer equations are

$$\frac{\partial u}{\partial t} + u\frac{\partial u}{\partial x} + v\frac{\partial u}{\partial y} = U_\infty \frac{\mathrm{d}U_\infty}{\mathrm{d}x} + \frac{\partial^2 u}{\partial y^2}, \tag{5}$$

$$\frac{\partial u}{\partial x} + \frac{\partial v}{\partial y} = 0, \tag{6}$$

where u is the velocity in the x-direction. The boundary conditions are

$$u = -1, \; v = 0 \quad \text{at} \quad y = 0; \quad u \to U_\infty(x) \quad \text{as} \quad y \to \infty, \tag{7}$$

where $U_\infty(x)$ is given by (4). For the limit problem $Re \to \infty$, the vortex is always located at $x = 0$, $Y = 1$ in the convected reference frame and the mainstream flow is steady. In part 2 of this study (Peridier, Smith & Walker 1991), interactive boundary-layer solutions at finite Re will be considered, where the thickening boundary layer alters the vortex trajectory and the external flow is therefore also unsteady.

The problem described by (4)–(7) was originally considered by Walker (1978) who assumed that the motion was initiated impulsively from rest. Numerical solutions for the developing boundary-layer flow were obtained in terms of a stream function $\Psi(x, \tilde{\eta}, t)$ defined by

$$u = -1 + U_e(x)\frac{\partial \Psi}{\partial \tilde{\eta}}. \tag{8}$$

Here $\tilde{\eta}$ is a Rayleigh variable defined by

$$\tilde{\eta} = y/2t^{\frac{1}{2}}, \tag{9}$$

which accounts for the fact that the boundary layer thickens proportional to $t^{\frac{1}{2}}$ after the impulsive start. The numerical results of Walker (1978) showed that a recirculating eddy developed in the boundary layer a short time after the start of the motion (at $t = 0.281$) as a consequence of the adverse pressure gradient imposed by the vortex. With the passage of time, the region of recirculation grew in both the streamwise and normal directions and eventually the boundary-layer flow entered a phase where rapid growth began to evolve on one side of the recirculating eddy. At this stage the displacement thickness distribution became almost vertical locally with an intense variation in the streamwise direction developing at this location. This behaviour is typically observed in unsteady boundary-layer flows which are proceeding toward a strong viscous–inviscid interaction with the external flow (see, for example, Doligalski & Walker 1984; Ece *et al.* 1984; Walker *et al.* 1987). It is characterized by a rapidly strengthening outflow from the boundary layer over a thin zone which progressively narrows in the streamwise direction (Van Dommelen & Shen 1982; Elliott *et al.* 1983; Cowley, Van Dommelen & Lam 1990). For this reason it proves impossible to adequately resolve such phenomena using a fixed mesh in the (x, y)-plane and the conventional Eulerian description of the flow. For the problem of interest here, it was difficult to continue the numerical integrations much beyond $t = 0.75$ with good accuracy using the Eulerian approach, despite various attempts to do so (Walker 1978). In the present study, Lagrangian variables were used to continue the numerical integrations up to the evolution of a singularity and the onset of interaction with the external flow.

In the Lagrangian description of the boundary-layer motion, the coordinates (ξ, η) of a large number of fluid particles at some initial instant in time are used as independent spatial variables. The current position of each fluid particle (x, y) (as well as its velocity components u, v) are functions of (ξ, η, t), corresponding to where the particle originally started and the elapsed time along its trajectory respectively. The transformation from Eulerian to Lagrangian coordinates is given by (Van Dommelen 1981; Peridier & Walker 1989)

$$\frac{\partial}{\partial x} = \frac{\partial y}{\partial \eta}\frac{\partial}{\partial \xi} - \frac{\partial y}{\partial \xi}\frac{\partial}{\partial \eta}, \quad \frac{\partial}{\partial y} = -\frac{\partial x}{\partial \eta}\frac{\partial}{\partial \xi} + \frac{\partial x}{\partial \xi}\frac{\partial}{\partial \eta}, \tag{10}$$

and the substantive derivative becomes a Lagrangian derivative in time. As originally pointed out by Van Dommelen & Shen (1980), the boundary-layer momentum equation corresponding to (5) is the system

$$\frac{\partial u}{\partial t} = U_\infty U'_\infty(x) + \left(\frac{\partial x}{\partial \xi}\frac{\partial}{\partial \eta} - \frac{\partial x}{\partial \eta}\frac{\partial}{\partial \xi}\right)^2 u, \tag{11}$$

$$\frac{\partial x}{\partial t} = u, \tag{12}$$

for the dependent variables $x(\xi, \eta, t)$ and $u(\xi, \eta, t)$, describing the current streamwise location and velocity of each fluid particle. In (11), $U_\infty(x)$ and its derivative are known functions of x obtained, in general, from a solution of the outer inviscid problem. The initial conditions for this system are that the streamwise velocity distribution is known at some initial instant $t = t_0$, namely

$$u = u_0(\xi, \eta) \quad \text{at} \quad t = t_0 \tag{13}$$

for known fluid particle locations in the boundary layer

$$x(\xi, \eta, t) = \xi, \quad y(\xi, \eta, t) = \eta \quad \text{at} \quad t = t_0. \tag{14}$$

The boundary conditions for (11) are that the streamwise velocity must match the mainstream for large η according to

$$u(\xi, \eta, t) \to U_\infty(x) \quad \text{as} \quad \eta \to \infty, \tag{15}$$

and that fluid particles originally on the wall remain there (in view of the no-slip condition), namely

$$u = -1 \quad \text{at} \quad \eta = 0. \tag{16}$$

One of the principal advantages of the Lagrangian description is that (11) and (12) do not contain the dependent variables corresponding to the normal particle positions y and velocities v; it is these quantities which become large (and eventually singular) as a boundary layer moves toward a strong interaction with the outer flow, thus giving rise to considerable difficulties in numerical solutions within the Eulerian formulation. By contrast, it is believed that the streamwise particle positions x and tangential velocities u remain regular (Van Dommelen 1981), even as the boundary layer evolves toward an eruption. The flow development is computed by advancing the solution of (11) and (12) forward in time numerically. At any stage, the normal distance $y(\xi, \eta, t)$ may be computed as a solution of the continuity equation

$$\frac{\partial x}{\partial \xi}\frac{\partial y}{\partial \eta} - \frac{\partial x}{\partial \eta}\frac{\partial y}{\partial \xi} = 1, \tag{17}$$

in Lagrangian coordinates. If at any time t the streamwise particle positions $x(\xi, \eta, t)$ are known from a numerical solution of the system (11) and (12), the normal positions $y(\xi, \eta, t)$ may be computed from (17) which is a first-order equation having the characteristics

$$\frac{\mathrm{d}\xi}{(-\partial x/\partial \eta)} = \frac{\mathrm{d}\eta}{\partial x/\partial \xi} = \mathrm{d}y, \tag{18}$$

which are curves of constant x. An integral of (18) is

$$y(\xi, \eta, t) = \int_{\text{wall}}^{(\xi, \eta)} \frac{\mathrm{d}s}{(x_\xi^2 + x_\eta^2)^{\frac{1}{2}}}, \tag{19}$$

where the integral is along a path of constant x which passes through the point (ξ, η), denoting a specific fluid particle; the lower limit on the integral in (19) corresponds to the location where the specific constant-x contour passing through (ξ, η) originates on the wall. Thus, the normal distance from the wall of a fluid particle at time t which started at (ξ, η) at some initial instant $t = t_0$ is given by (19). It is evident that if a stationary point develops in the x-field at some subsequent time t_s, namely

$$\frac{\partial x}{\partial \xi} = \frac{\partial x}{\partial \eta} = 0 \quad \text{at} \quad \xi = \xi_s, \quad \eta = \eta_s \quad \text{at} \quad t = t_s, \tag{20}$$

then (19) shows that a singularity has evolved in the boundary-layer solution. In physical terms, (17) expresses conservation of mass and when a stationary point in the x-field develops, the implication is that the fluid particle which started at (ξ_s, η_s) has been compressed to zero thickness in the streamwise direction. By continuity, the fluid particle must then grow substantially in a direction normal to the wall.

Since the boundary-layer equations do not contain terms describing the influence of normal pressure gradients and viscous diffusion, there is no resistance to this distortion (Cowley *et al.* 1990) and a portion of the fluid particle is therefore ultimately located at an infinite distance from the wall. Consequently, the normal velocity is also singular at this streamwise location and as the boundary layer erupts (over a region of zero streamwise thickness), fluid particles above the flattened particle that originated at (ξ_s, η_s) are thrown out into the inviscid region.

3. Transformation to a finite domain

In a numerical solution of the boundary-layer problem in Lagrangian coordinates, it is convenient to work in terms of independent variables defined on a finite range as well as a dependent variable which ranges from 0 to 1 across the boundary layer. A new independent variable is defined by

$$u(\xi, \eta, t) = -1 + U_e(x)\, U(\xi, \eta, t), \tag{21}$$

where U_e is defined by (4). To satisfy conditions (7), the function U must satisfy

$$U(\xi, 0, t) = 0 \quad \lim_{\eta \to \infty} U(\xi, \eta, t) = 1. \tag{22}$$

The independent variable ξ is defined on the range $(-\infty, \infty)$ but may be transformed to the finite range $(2, 0)$ by the Görtler-type transformation (Walker 1978)

$$\hat{\xi} = 1 - \frac{2}{\pi} \arctan \xi. \tag{23}$$

In this new coordinate, $\hat{\xi} = 0$ corresponds to upstream infinity, $\hat{\xi} = 1$ to the streamwise location of the vortex centre and $\hat{\xi} = 2$ to downstream infinity. A similar transformation may also be adopted for the dependent variable $x(\xi, \eta, t)$ to yield a new variable $\hat{x}$, again defined on the range $(2, 0)$ according to

$$\hat{x} = 1 - \frac{2}{\pi} \arctan x. \tag{24}$$

In terms of $\hat{x}$, the mainstream velocity function defined in (4) becomes

$$U_e(\hat{x}) = 2(1 - \cos \pi \hat{x}). \tag{25}$$

Lastly, the independent variable η is defined on the range $(0, \infty)$ and a convenient mapping to the finite range $(0, 1)$ is

$$\hat{\eta} = \frac{2}{\pi} \arctan \eta. \tag{26}$$

When the transformations (21), (23), (24) and (26) are made in the Lagrangian boundary-layer equations (11) and (12), it may be shown that the equations for U and $\hat{x}$ are of the form

$$\frac{\partial U}{\partial t} = R \frac{\partial^2 U}{\partial \hat{\xi}^2} + S \frac{\partial^2 U}{\partial \hat{\xi}\, \partial \hat{\eta}} + T \frac{\partial^2 U}{\partial \hat{\eta}^2} + P \frac{\partial U}{\partial \hat{\eta}} + Q \frac{\partial U}{\partial \hat{\xi}} + WU + \Gamma, \tag{27}$$

$$\frac{\partial \hat{x}}{\partial t} = \frac{U_e(\hat{x})}{2\pi} \{1 - U_e(\hat{x})\, U(\hat{\xi}, \hat{\eta}, t)\}. \tag{28}$$

The functional coefficients in (27) are defined by

$$R = \alpha^2\left(\frac{\partial\hat{x}}{\partial\hat{\eta}}\right)^2, \quad S = -2\alpha^2\left(\frac{\partial\hat{x}}{\partial\hat{\eta}}\right)\left(\frac{\partial\hat{x}}{\partial\hat{\xi}}\right), \quad T = \alpha^2\left(\frac{\partial\hat{x}}{\partial\hat{\xi}}\right)^2, \tag{29}$$

$$P = \alpha^2\left\{\frac{\partial\hat{x}}{\partial\hat{\xi}}\left(\frac{\partial^2\hat{x}}{\partial\hat{\xi}\,\partial\hat{\eta}}+\beta(\hat{\eta})\frac{\partial\hat{x}}{\partial\hat{\xi}}\right)-\frac{\partial\hat{x}}{\partial\hat{\eta}}\left(\frac{\partial^2\hat{x}}{\partial\hat{\xi}^2}+\gamma(\hat{\xi})\frac{\partial\hat{x}}{\partial\hat{\xi}}\right)\right\}, \tag{30}$$

$$Q = \alpha^2\left\{\frac{\partial\hat{x}}{\partial\hat{\eta}}\left(\frac{\partial^2\hat{x}}{\partial\hat{\eta}\,\partial\hat{\xi}}+\gamma(\hat{\xi})\frac{\partial\hat{x}}{\partial\hat{\eta}}\right)-\frac{\partial\hat{x}}{\partial\hat{\xi}}\left(\frac{\partial^2\hat{x}}{\partial\hat{\eta}^2}+\beta(\hat{\eta})\frac{\partial\hat{x}}{\partial\hat{\eta}}\right)\right\}, \tag{31}$$

$$W = -\frac{1}{2\pi}\{1-U_e(\hat{x})\,U(\hat{\xi},\hat{\eta},t)\}\,U_e'(\hat{x}), \tag{32}$$

$$\Gamma = \frac{1}{2\pi}\{1-U_e(\hat{x})\}\,U_e'(\hat{x}). \tag{33}$$

In these equations, a prime denotes an ordinary derivative with respect to the indicated variable and $\alpha(\hat{x},\hat{\xi},\hat{\eta})$, $\beta(\hat{\eta})$ and $\gamma(\hat{\xi})$ are defined by

$$\alpha(\hat{x},\hat{\xi},\hat{\eta}) = U_e(\hat{\xi})\,Z(\hat{\eta})/U_e(\hat{x}), \tag{34}$$

$$\beta(\hat{\eta}) = Z'(\hat{\eta})/Z(\hat{\eta}), \quad \gamma(\hat{\xi}) = U_e'(\hat{\xi})/U_e(\hat{\xi}), \tag{35}$$

where

$$Z(\hat{\eta}) = (1+\cos\pi\hat{\eta})/\pi \tag{36}$$

and U_e is given by (25).

In the present study, the boundary-layer development was calculated by computing the initial development after the impulsive start using a conventional Eulerian formulation in the manner described by Walker (1978). At a selected time $t = t_0$, the calculation was switched to the Lagrangian formulation. The initial conditions for (27) and (28) are

$$\hat{x} = \hat{\xi}, \quad U = U_0(\hat{\xi},\hat{\eta}) \quad \text{at} \quad t = t_0, \tag{37}$$

where U_0 may be evaluated at each nodal point from the Eulerian solution (carried up to the switch time t_0); alternatively, if the Lagrangian formulation is used starting at the impulsive start at $t = 0$, $U_0 = 1$. Boundary conditions for the system (27) and (28) for $t > t_0$ are

$$U(\hat{\xi},0,t) = 0, \quad U(\hat{\xi},1,t) = 1, \tag{38}$$

$$\hat{x}(0,\hat{\eta},t) = 0, \quad \hat{x}(2,\hat{\eta},t) = 2. \tag{39}$$

The conditions (39) state that fluid particles which are initially at downstream or upstream infinity remain there. The $\hat{x}$ particle positions along the wall and at the mainstream may be obtained at any value of t through integration of (28) using (38). Fluid particles on the wall (or at an infinite distance from the wall) remain there but their streamwise positions change with time. It is possible to obtain analytical solutions for $\hat{x}$ on the wall and at the mainstream and, for example,

$$\hat{x}(\hat{\xi},0,t) = 1-\frac{2}{\pi}\arctan\left\{\tan\frac{\pi(1-\hat{\xi})}{2}-(t-t_0)\right\}, \tag{40}$$

on the wall. Finally, at upstream and downstream infinity, the coefficients in (27) assume limiting forms independent of t and it can be shown that

$$U(\hat{\xi},\hat{\eta},t) = \operatorname{erf}\left\{\frac{\tan\frac{1}{2}\pi\hat{\eta}}{2t^{\frac{1}{2}}}\right\} \quad \text{at} \quad \hat{\xi} = 0,2. \tag{41}$$

This completes the formulation of the boundary-layer problem in Lagrangian variables and the numerical solution procedure used to solve (27) and (28) is described in the next section.

4. Numerical methods

The form of the boundary-layer equation (27) in Lagrangian variables is similar to the corresponding form in the Eulerian description (Walker 1978) in that both are second-order parabolic partial differential equations. However, the characteristic behaviour of the resulting difference equations was found to be quite different. In the standard Crank–Nicolson procedure (Walker 1978), (27) is approximated midway between the current and previous time plane and spatial derivatives are approximated by conventional central differences. In this manner a set of nonlinear difference equations is obtained at each internal meshpoint. A conventional method of solving this equation consists of a systematic point-by-point sweep of the mesh at each time step. This procedure works very well for calculations based on the Eulerian description of the motion (Walker 1978) but failed to converge when applied to the Lagrangian equations, as soon as significant updraughts began to develop in the boundary-layer flow (Peridier & Walker 1989). Although it was found that the convergence could be enhanced somewhat by altering the pattern in which the mesh was swept, the conventional Crank–Nicolson method was considered too time consuming and abandoned (see also Van Dommelen 1981).

Another popular approach that was also unsuccessful in the present application is the factored alternating-direction method due to Beam & Warming (1978). In this algorithm, (27) is factored into two operators on U, one in each of the $\hat{\xi}$- and $\hat{\eta}$-directions. A sequence of tridiagonal problems, along lines of constant $\hat{\xi}$ and then lines of constant $\hat{\eta}$ (or vice versa) is computed at each time step. The Beam & Warming (1978) algorithm is explicit in the sense that calculations involve only one sweep in each coordinate direction and iteration is not carried out at each time step. In the present study, the Beam & Warming algorithm was found to work well at early times and to produce answers consistent with the conventional Crank–Nicolson method. However, at subsequent times the method produced results, which upon close examination of the contours of constant $\hat{x}$ and U, were judged to be erroneous. The failure of the method is believed due to the fact that, as strong updraughts begin to develop in the boundary layer, the tridiagonal problems in each of the coordinate directions eventually lose the property of diagonal dominance, and this results in a numerical instability in the method. It should be noted that the Beam & Warming (1978) algorithm is commonly applied to time-dependent problems in which the objective is to compute the flow evolution through to steady state and for which the level of time-dependence is continually diminishing. In the present application the reverse situation applies and variations in time become progressively more intense as the boundary layer evolves toward an eruption.

In view of the failure of conventional numerical procedures, which had previously worked well in Eulerian formulations, it was necessary to develop an alternative procedure. The method described here is a factored ADI (Alternating-Direction-Implicit) scheme in which 'upwind-downwind' differencing of the first-order partial derivatives was carried out to ensure that the tridiagonal matrix problems in each of the coordinate directions were diagonally dominant. The method is second-order accurate in both spatial directions and in time and was found to be very effective in calculating the solution of the Lagrangian boundary-layer equations, particularly in

the latter stages of the integrations, when convection effects are dominant in a locally eruptive zone and where the coefficients of the first derivatives in (27) become large. To describe the progress of the algorithm through a time step, assume that the solution for U is desired at time t and that the solution in the previous time plane (denoted by U^*) at time $t^* = t - \Delta t$ is known. Suppose that the spatial domain $(\hat{\xi}, \hat{\eta})$ is subdivided in a mesh with $(M-1)$ and $(N-1)$ equal intervals in the $\hat{\xi}$- and $\hat{\eta}$-directions respectively and let subscripts i,j denote functional values at a typical point in the mesh at $(\hat{\xi}_i, \hat{\eta}_j)$. Equation (27) is first approximated at the typical point in the mesh midway between the current and previous time plane at $\bar{t} = t^* + (\frac{1}{2}\Delta t)$ to obtain

$$\frac{U_{i,j} - U^*_{i,j}}{\Delta t} = \bar{\Gamma}_{i,j} + \left\{ \bar{R}_{i,j} \frac{\partial^2}{\partial \hat{\xi}^2} + \bar{S}_{i,j} \frac{\partial^2}{\partial \hat{\xi} \partial \hat{\eta}} + \bar{T}_{i,j} \frac{\partial^2}{\partial \hat{\eta}^2} + \bar{P}_{i,j} \frac{\partial}{\partial \hat{\eta}} + \bar{Q}_{i,j} \frac{\partial}{\partial \hat{\xi}} + \bar{W}_{i,j} \right\} \bar{U}_{i,j}, \quad (42)$$

which is accurate to $O(\Delta t^2)$. Here $\bar{U}_{i,j}$ denotes the simple average

$$\bar{U}_{i,j} = \tfrac{1}{2}(U_{i,j} + U^*_{i,j}). \quad (43)$$

In (42) the overbar denotes quantities evaluated at $\bar{t}$ which may be related to the corresponding terms in the previous and current time planes by a simple average, and

$$\bar{P}_{i,j} = \tfrac{1}{2}(P_{i,j} + P^*_{i,j}), \quad (44)$$

for example. It may be noted from (29)–(32) that the quantities $R_{i,j}$, $S_{i,j}$, $T_{i,j}$, $P_{i,j}$, $Q_{i,j}$, and $W_{i,j}$ depend on $U_{i,j}$, and in the present approach are treated as known distributions which are updated continually as an iteration takes place at each time step.

In a conventional Crank–Nicolson approach, the spatial derivatives in (42) are evaluated using central differences and the resulting difference equations are solved iteratively for the $U_{i,j}$. However, when $\bar{P}_{i,j}$ and $\bar{Q}_{i,j}$ become large locally, the matrix problem can suffer a loss of diagonal dominance which may lead to divergence of the iteration. To overcome this problem, 'upwind-downwind' differencing may be used for the first-derivative terms in the manner described by Doligalski & Walker (1978, 1984) (see also Van Dommelen & Shen 1980) wherein, for example,

$$\bar{P}_{i,j} \frac{\partial \bar{U}_{i,j}}{\partial \hat{\eta}} = \frac{1}{2\Delta \hat{\eta}} \bar{P}_{i,j} \begin{cases} U_{i,j+1} - U_{i,j} + U^*_{i,j} - U^*_{i,j-1} & \text{if } \bar{P}_{i,j} > 0, \\ U_{i,j} - U_{i,j-1} + U^*_{i,j+1} - U^*_{i,j} & \text{if } \bar{P}_{i,j} < 0. \end{cases} \quad (45)$$

This approximation is second-order accurate in both Δt and $\Delta \hat{\eta}$ and acts to enhance the diagonal dominance of the system of difference equations. The approximation in (45) slants between the current and previous time plane in a manner dependent on the local sign of the coefficient $\bar{P}_{i,j}$. A similar approximation can also be made for $\bar{Q}_{i,j}$ $(\partial \bar{U}_{i,j}/\partial \hat{\xi})$ which depends on the local sign of $\bar{Q}_{i,j}$. To facilitate the factoring of the difference equations, it is convenient to express the upwind-downwind differencing in a compact form (Peridier & Walker 1988) by introducing the operators $\chi^+_{\hat{\eta}}$, $\chi^-_{\hat{\eta}}$, $\chi^+_{\hat{\xi}}$, $\chi^-_{\hat{\xi}}$ defined by

$$\chi^+_{\hat{\eta}} = \delta_{\hat{\eta}} \mathrm{E}^{\frac{1}{2}\mathrm{sgn}(\bar{P}_{i,j})}_{\hat{\eta}}, \quad \chi^-_{\hat{\eta}} = \delta_{\hat{\eta}} \mathrm{E}^{-\frac{1}{2}\mathrm{sgn}(\bar{P}_{i,j})}_{\hat{\eta}} \quad (46)$$

$$\chi^+_{\hat{\xi}} = \delta_{\hat{\xi}} \mathrm{E}^{\frac{1}{2}\mathrm{sgn}(\bar{Q}_{i,j})}_{\hat{\xi}}, \quad \chi^-_{\hat{\xi}} = \delta_{\hat{\xi}} \mathrm{E}^{-\frac{1}{2}\mathrm{sgn}(\bar{Q}_{i,j})}_{\hat{\xi}}. \quad (47)$$

Here $\mathrm{E}_{\hat{\xi}}$ and $\mathrm{E}_{\hat{\eta}}$ are the finite-difference enlargement operators in each of the coordinate directions given by

$$\mathrm{E}^{\pm\frac{1}{2}}_{\hat{\xi}} U(\hat{\xi}, \hat{\eta}) = U(\hat{\xi} \pm \tfrac{1}{2}\Delta \hat{\xi}, \hat{\eta}), \quad \mathrm{E}^{\pm\frac{1}{2}}_{\hat{\eta}} U(\hat{\xi}, \hat{\eta}) = U(\hat{\xi}, \hat{\eta} \pm \tfrac{1}{2}\Delta \hat{\eta}) \quad (48)$$

(as described in the Appendix) and $\delta_{\hat{\xi}}$ and $\delta_{\hat{\eta}}$ are the central-difference operators

$$\delta_{\hat{\xi}} = \mathrm{E}_{\hat{\xi}}^{\frac{1}{2}} - \mathrm{E}_{\hat{\xi}}^{-\frac{1}{2}}, \quad \delta_{\hat{\eta}} = \mathrm{E}_{\hat{\eta}}^{\frac{1}{2}} - \mathrm{E}_{\hat{\eta}}^{-\frac{1}{2}}. \tag{49}$$

In addition, the function sgn (x) is either 1 or -1 depending on whether x is positive or negative respectively. In terms of the operators defined by (46) and (47), the upwind-downwind differencing for the first derivatives in (42) may be written

$$\bar{P}_{i,j} \frac{\partial \bar{U}_{i,j}}{\partial \hat{\eta}} = \frac{1}{2\Delta\hat{\eta}} \bar{P}_{i,j} \{\chi_{\hat{\eta}}^{+} U_{i,j} + \chi_{\hat{\eta}}^{-} U_{i,j}^{*}\}, \tag{50}$$

$$\bar{Q}_{i,j} \frac{\partial \bar{U}_{i,j}}{\partial \hat{\xi}} = \frac{1}{2\Delta\hat{\xi}} Q_{i,j} \{\chi_{\hat{\xi}}^{+} U_{i,j} + \chi_{\hat{\xi}}^{-} U_{i,j}^{*}\}. \tag{51}$$

The remaining second-derivative terms in (42) were approximated using the usual central-difference expressions according to

$$\frac{\partial^2 \bar{U}_{i,j}}{\partial \hat{\eta}^2} = \frac{1}{2(\Delta\hat{\eta})^2} \{\delta_{\hat{\eta}}^2 (U_{i,j} + U_{i,j}^{*})\}, \tag{52}$$

$$\frac{\partial^2 \bar{U}_{i,j}}{\partial \hat{\xi}^2} = \frac{1}{2(\Delta\hat{\xi})^2} \{\delta_{\hat{\xi}}^2 (U_{i,j} + U_{i,j}^{*})\}, \tag{53}$$

$$\frac{\partial^2 \bar{U}_{i,j}}{\partial \hat{\xi} \partial \hat{\eta}} = \frac{1}{2(\Delta\hat{\xi})(\Delta\hat{\eta})} \{\mu_{\hat{\eta}} \delta_{\hat{\eta}} \mu_{\hat{\xi}} \delta_{\hat{\xi}} (U_{i,j} + U_{i,j}^{*})\}. \tag{54}$$

Here $\mu_{\hat{\xi}}$ and $\mu_{\hat{\eta}}$ are the averaging central-difference operators defined by

$$\mu_{\hat{\xi}} = \tfrac{1}{2}\{\mathrm{E}_{\hat{\xi}}^{\frac{1}{2}} + \mathrm{E}_{\hat{\xi}}^{-\frac{1}{2}}\}, \quad \mu_{\hat{\eta}} = \tfrac{1}{2}(\mathrm{E}_{\hat{\eta}}^{\frac{1}{2}} + \mathrm{E}_{\hat{\eta}}^{-\frac{1}{2}}). \tag{55}$$

Upon substitution of (50)–(55) into (42) and factoring the spatial-difference operators, it can be shown that

$$\left\{1 - \frac{\mathrm{w}_{i,j}}{(\Delta\hat{\xi})^2} (\bar{R}_{i,j} \delta_{\hat{\xi}}^2 + (\Delta\hat{\xi}) \bar{Q}_{i,j} \chi_{\hat{\xi}}^{+})\right\} \left\{1 - \frac{\mathrm{w}_{i,j}}{(\Delta\hat{\eta})^2} (\bar{T}_{i,j} \delta_{\hat{\eta}}^2 + (\Delta\hat{\eta}) \bar{P}_{i,j} \chi_{\hat{\eta}}^{+})\right\} U_{i,j} = D_{i,j}, \tag{56}$$

where

$$\mathrm{w}_{i,j} = \frac{\Delta t}{2 - \bar{W}_{i,j} \Delta t} \tag{57}$$

and

$$D_{i,j} = 2\mathrm{w}_{i,j} \frac{U_{i,j}^{*}}{\Delta t} + \mathrm{w}_{i,j} \left\{\bar{W}_{i,j} + \frac{\bar{P}_{i,j}}{\Delta\hat{\eta}} \chi_{\hat{\eta}}^{-} + \frac{\bar{T}_{i,j}}{(\Delta\hat{\eta})^2} \delta_{\hat{\eta}}^2 + \frac{\bar{R}_{i,j}}{(\Delta\hat{\xi})^2} \delta_{\hat{\xi}}^2 + \frac{\bar{Q}_{i,j}}{\Delta\hat{\xi}} \chi_{\hat{\xi}}^{-}\right\} U_{i,j}^{*}$$
$$+ \mathrm{w}_{i,j} \left\{2\bar{\Gamma}_{i,j} + \frac{\bar{S}_{i,j}}{(\Delta\hat{\xi})(\Delta\hat{\eta})} \mu_{\hat{\xi}} \delta_{\hat{\xi}} \mu_{\hat{\eta}} \delta_{\hat{\eta}} (U_{i,j} + U_{i,j}^{*})\right\}. \tag{58}$$

Two points should be noted. First, (56) is not identical to (42) and differs by a term $O(\Delta t^2)$; however, this latter error is of the same order of magnitude as incurred in the original difference approximation (42) and may thus be neglected. Secondly, $D_{i,j}$ generally involves differences of known quantities in the previous time plane, with the exception of the last term in (58) which arises from the approximation to the cross-derivative $\partial^2 U / \partial\hat{\xi}\partial\hat{\eta}$; the difference approximations to this term are not easily factored and were evaluated on the right-hand side of (56) as part of a general iterative procedure at each time step.

Equation (56) can be solved as an ordered sequence of tri-diagonal matrix problems by introducing an intermediate variable $\tilde{U}_{i,j}$ such that

$$\left\{1-\frac{\mathrm{w}_{i,j}}{(\Delta\hat{\xi})^2}\{\bar{R}_{i,j}\delta_{\hat{\xi}}^2+(\Delta\hat{\xi})\bar{Q}_{i,j}\chi_{\hat{\xi}}^{\pm}\}\right\}\tilde{U}_{i,j}=D_{i,j}, \tag{59}$$

$$\left\{1-\frac{\mathrm{w}_{i,j}}{(\Delta\hat{\eta})^2}\{\bar{T}_{i,j}\delta_{\hat{\eta}}^2+(\Delta\hat{\eta})\bar{P}_{i,j}\chi_{\hat{\eta}}^{+}\}\right\}U_{i,j}=\tilde{U}_{i,j}. \tag{60}$$

To initiate an iterative solution for $U_{i,j}$ in the current time plane, (60) was used to provide values of $\tilde{U}_{i,j}$ on $\hat{\xi}=0,2$ and (59) was then solved systematically along lines of constant $\hat{\eta}$ using the Thomas algorithm to provide a direct solution for each tridiagonal problem for $\tilde{U}_{i,j}$. Upon completion of the first sweep of the mesh, the sequence of tridiagonal problems defined by (60) was solved along lines of constant $\hat{\xi}$. This second sweep of the mesh completed the first iteration for $U_{i,j}$ and the streamwise particle positions in the current time place were estimated from the difference approximation to (28).

$$\hat{x}_{i,j}=x_{i,j}^{*}+\frac{\Delta t}{2\pi}U_{\mathrm{e}}(\bar{\hat{x}}_{i,j})\{1-U_{\mathrm{e}}(\bar{\hat{x}}_{i,j})\bar{U}_{i,j}\}, \tag{61}$$

Here $\bar{U}_{i,j}$ is given by (43) and

$$\bar{\hat{x}}_{i,j}=\tfrac{1}{2}(\hat{x}_{i,j}+\hat{x}_{i,j}^{*}). \tag{62}$$

Note that at the first iteration, $\hat{x}_{i,j}$ in (62) and $U_{i,j}$ in (43) were approximated by the corresponding quantities in the previous time plane. Once each iteration was completed, the coefficients in the momentum equation (27), $R_{i,j}$, $S_{i,j}$, $T_{i,j}\ldots$ given by (29)–(32) were updated. The entire process was then repeated until successive iterates of $U_{i,j}$ converged at every node with a relative error of less than 10^{-4}, at which point the integration was advanced to the next time plane. Although testing for convergence on $\hat{x}_{i,j}$ was also carried out, this is generally not necessary and agreement to four significant figures in U is normally a sufficient indication of overall convergence. It is noted in passing that a line iteration technique similar to the present ADI method was used in a Lagrangian calculation by Lam (1988).

Numerical solutions were obtained in both the Eulerian and Lagrangian systems. The calculations were started at $t=0$ with an impulsive start condition and initially were advanced in time using the Eulerian formulation described by Walker (1978). At $t=t_0$, the computed streamwise velocity distribution was used to initiate an integration in Lagrangian variables forward in time. Various values of t_0 were used as a check on the accuracy (including $t_0=0$) in order to cross-compare the results of the two integration methods; as expected, the specific value of t_0 had no effect on the actual computed results. The time $t_0=0.25$ is a convenient point to switch, since the normal coordinate y is equivalent to the Rayleigh variable (9) at that time. In addition, the Eulerian integration can be continued to around $t=0.7$ without difficulty (Walker 1978), and thus a switch at $t_0=0.25$ provides a good intermediate range to compare the results of both integration procedures. Calculations in the Lagrangian frame can be continued until $t_{\mathrm{s}}=0.989$ when a singularity develops in the boundary-layer solution; in fact, it is possible to continue the numerical integrations for $t>t_{\mathrm{s}}$ in the Lagrangian coordinates even though such results are not physically meaningful. Solutions were carried out for three sets of mesh sizes which are summarized in table 1; here, for example, 201×101 implies that there is a total

Time	Mesh 1 (61 × 41)	Mesh 2 (101 × 61)	Mesh 3 (201 × 101)
0.2500	0.0100	0.0010	0.0010
0.5500	0.0010	0.0010	0.0010
0.7500	0.0010	0.0010	0.0005
0.8250	0.0010	0.0010	0.0002
0.8600	0.0005	0.0005	0.0002
0.9500	0.0005	0.0005	0.0001

TABLE 1. Time steps used in the integrations; the Eulerian method was used up to $t = 0.25$ and the Lagrangian method thereafter. The entries indicate the time step Δt initiated at the given time.

of 201 and 101 points in the $\hat{\xi}$- and $\hat{\eta}$-directions respectively. The calculated results were in good agreement between three sets of meshes. One feature of the Lagrangian equations is that as the spatial mesh size is reduced, it is necessary to decrease the time step as indicated in table 1 in order to avoid stability problems. It should be noted that when numerical instabilities do develop in the Lagrangian integrations a catastrophic failure of the algorithm does not occur. Rather the integrations proceed in an apparently normal manner. In the present study, contours of constant $\hat{x}$ and U were plotted periodically during the course of the integrations to ensure smoothness in the results. When physically unrealistic 'wiggles' in the contours were noted, the calculations were started at an earlier time with a reduced time step. The time steps listed in table 1 were determined in this manner. Consequently, the onset of numerical instabilities was suppressed in this study by trial and error and by taking very small time steps. Unfortunately, a way of automatically selecting the time step was not found, and thus there was essentially no immediate warning when a problem started to occur in the integrations; eventually the number of iterations at each time step does start to increase when instabilities occur, but this is usually many time steps after the first appearance of 'wiggles' in the computed results. Lastly, it should be noted that as the boundary layer starts to focus toward an eruption in the final stages of the integrations, a severe reduction in the time step is generally necessary.

5. Evolution of the singularity

A revealing feature of the developing boundary layer in Lagrangian coordinates is the behaviour of the contours of constant x, or equivalently constant $\hat{x}$. As discussed in §2, a singularity occurs in the boundary-layer solution when the x-field develops a stationary point according to (20); in terms of the variables defined in (23), (24) and (26), a stationary point occurs at $t = t_s$ when

$$\frac{\partial \hat{x}}{\partial \hat{\xi}} = \frac{\partial \hat{x}}{\partial \hat{\eta}} = 0 \quad \text{at} \quad \hat{\xi} = \hat{\xi}_s, \hat{\eta} = \hat{\eta}_s. \tag{63}$$

At the initiation of the Lagrangian calculation $\hat{x} = \hat{\xi}$, and it is of interest to determine how the condition (63) eventually evolves. In figure 2(*a*) the contours of constant $\hat{x}$ are plotted at $t = 0.45$. The specific values of $\hat{x}$ are not important in figure 2 but the shapes of the contours are. At the initiation of the Lagrangian integration at $t_0 = 0.25$, each constant $\hat{x}$-contour is a vertical straight line; by $t = 0.45$ these lines have distorted to the pattern shown in figure 2(*a*). The physical interpretation of these contours is that they represent the initial location of a line of fluid particles which at

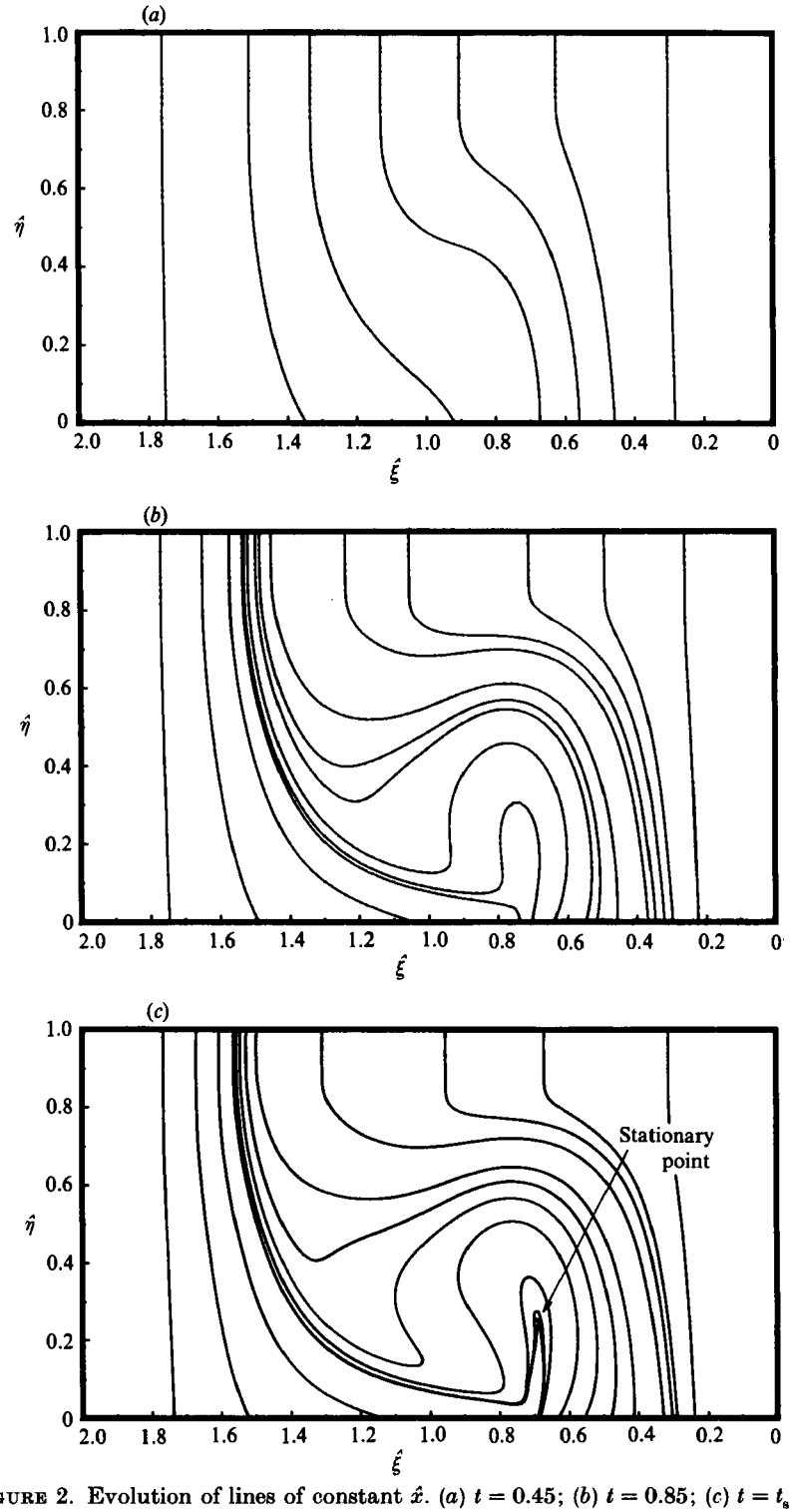

FIGURE 2. Evolution of lines of constant $\hat{x}$. (a) $t = 0.45$; (b) $t = 0.85$; (c) $t = t_s = 0.989$.

this time have now all arrived at constant x. Fluid particles on the wall remain there and are transported to the left with constant velocity -1 (in the convected frame). Far from the vortex, $U_e \to 0$ as $\hat{\xi} \to 0, 2$ and the fluid particles experience an almost constant drift to the left; thus, the constant $\hat{x}$ contours are almost straight lines. On the other hand, in the region near the vortex centre at $\hat{\xi} = 1$, the constant-$\hat{x}$ contours show considerable distortion and indicate that the fluid particles have experienced a drift to the right in the interval from $t = 0.25$ to $t = 0.45$, which is most pronounced in the upper part of the boundary layer. This behaviour is expected due to the action of the vortex above. As t increases, the trends noted in figure 2(*a*) continue as indicated in figure 2(*b*) at $t = 0.85$. Here it may be observed that a small 'thumb-like' region has formed which may only be accessed by constant-$\hat{x}$ contours that originate on the wall in a very narrow range near $\hat{\xi} = 0.75$. It is within this 'thumb' that a stationary point finally develops at $t_s = 0.989$ at the location shown in figure 2(*c*).

One advantage of the Lagrangian formulation is that the criterion (20) or (63) for the formation of a singularity is well defined. At the same time there are a number of practical difficulties associated with accurately estimating where and when in (ξ, η) – space the singularity actually occurs. In this study, the value of t_s was estimated by tracking the minimum of a gradient-norm function

$$\mathscr{N} = \left(\frac{\partial \hat{x}}{\partial \hat{\xi}}\right)^2 + \left(\frac{\partial \hat{x}}{\partial \hat{\eta}}\right)^2, \tag{64}$$

which must tend to zero as $t \to t_s$, and also by determining when the position of this minimum intersected the zero-vorticity line. Initially $\mathscr{N}$ is unity everywhere, but with increasing t an absolute minimum developed in the $\mathscr{N}$-distribution which was subsequently observed to decrease monotonically. At each time step, the $\mathscr{N}$-distribution was evaluated numerically using conventional central-difference approximations and the mesh point where $\mathscr{N}$ was a minimum was located. The precise location of the absolute minimum was located by representing the surface locally as a paraboloid (Peridier & Walker 1989) and locating the coordinates of the minimum $(\hat{\xi}_M, \hat{\eta}_M)$ using the conditions

$$\frac{\partial \mathscr{N}}{\partial \hat{\xi}} = \frac{\partial \mathscr{N}}{\partial \hat{\eta}} = 0 \quad \text{at} \quad \hat{\xi} = \hat{\xi}_M, \; \hat{\eta} = \hat{\eta}_M. \tag{65}$$

This procedure accurately evaluates $(\hat{\xi}_M, \hat{\eta}_M)$ at each time t and eventually gives the location of $(\hat{\xi}_s, \hat{\eta}_s)$ as $t \to t_s$. However, it is difficult to estimate the value of t_s using only this approach for the following reason. The quantity $\mathscr{N}$ is, by definition, non-negative for all t and the singularity occurs when the $\mathscr{N}$-surface first touches the plane $\mathscr{N} = 0$. However, because the gradients in (64) were evaluated numerically, they are never identically zero owing to discretization error. In practice, the minimum in $\mathscr{N}$ was observed to decrease monotonically but never quite reach zero. At a certain stage, the $\mathscr{N}$-surface started to flatten near $(\hat{\xi}_M, \hat{\eta}_M)$ and thereafter a spreading zone of almost zero $\mathscr{N}$ was noted. In fact, it appeared to be possible to continue the Lagrangian integrations well beyond the stage when it was suspected that a singularity has developed. For this reason, it is important to introduce an additional criterion to determine t_s.

The vorticity $\omega = -\partial u/\partial y$, and in Lagrangian coordinates

$$\omega = -\frac{\partial u}{\partial y} = \frac{\partial x}{\partial \eta}\frac{\partial u}{\partial \xi} - \frac{\partial x}{\partial \xi}\frac{\partial u}{\partial \eta}. \tag{66}$$

In terms of the present variables

$$\omega = U_e(\hat{\xi})\, Z(\hat{\eta}) \left\{ \frac{\partial \hat{x}}{\partial \hat{\eta}} \frac{\partial U}{\partial \hat{\xi}} - \frac{\partial \hat{x}}{\partial \hat{\xi}} \frac{\partial U}{\partial \hat{\eta}} \right\}. \tag{67}$$

In accordance with the MRS model, the singularity is expected to form on the zero-vorticity line at a finite time, and it is evident from (20), (63), (66) and (67) that $\omega = 0$ at the singular location. In the present problem the adverse pressure gradient due to the vortex induces a region of recirculating flow in the boundary layer at $t = 0.281$, and thereafter a line of zero vorticity is present within the boundary-layer flow. The singularity is expected to form somewhere along this line, and it is possible to identify t_s as that time when the absolute minimum in $\mathcal{N}$ at $(\hat{\xi}_M, \hat{\eta}_M)$ is located on the line $\omega = 0$. To locate the zero-vorticity line at any time t, the vorticity at each node in the mesh was computed from (67) using second-order-accurate central-difference formulae. A set of points (or, alternatively, fluid particles) $(\hat{\xi}, \hat{\eta})_k$ where $\omega = 0$ was then obtained by systematically sweeping the mesh along lines of constant $\hat{\xi}$ and constant $\hat{\eta}$ and using linear interpolation. The fluid particle closest to the particle $(\hat{\xi}_M, \hat{\eta}_M)$ at the minimum in $\mathcal{N}$ was then determined. The distance between these two points was observed to decrease monotonically to very small values as $t \to t_s$. Using this criterion, it proved possible to obtain a reliable estimate of t_s. Thus, near the end of the integration

$$(\hat{\xi}_M, \hat{\eta}_M) \to (\hat{\xi}_s, \hat{\eta}_s) \quad \text{as} \quad t \to t_s. \tag{68}$$

Here $(\hat{\xi}_s, \hat{\eta}_s)$, or equivalently (ξ_s, η_s), denotes the specific fluid particle which becomes squashed in the streamwise direction and in the process extends an infinite distance from the wall (on the boundary-layer scale) as the eruption develops. The normalized velocity U_s of this fluid particle is then easily evaluated from the numerical solution (Peridier & Walker 1989).

The best estimate of t_s is based on the smallest set of mesh sizes used (see table 1) and

$$t_s = 0.989, \tag{69}$$

which is also consistent with the values obtained with the other two meshes. Note that a larger (and incorrect) value of t_s was reported in the preliminary results of Peridier, Smith & Walker (1988). The best estimate of the streamwise location of the singularity is at $\hat{x}_s = 1.134$ or in terms of the physical coordinate x,

$$x_s = -0.214, \tag{70}$$

which is therefore to the left of the vortex centre. Elliott *et al.* (1983) use the notation

$$u = -K \tag{71}$$

to denote the velocity of the squashed fluid particle at the eruption time. A positive value of K implies that, for a stationary wall, the separation is moving upstream; for the impulsively started circular cylinder, Van Dommelen & Shen (1980) found $K = 0.26$ and classified the situation as 'upstream-slipping separation'. In the present problem, the wall moves continuously upstream in the vortex frame and the streamwise velocities are relative to this frame. The value of K is calculated from

$$-K = -1 + U_e(\hat{x}_s)\, U_s, \tag{72}$$

where U_s is the independent variable U evaluated at (ξ_s, η_s) at $t = t_s$. The best estimate for K is

$$K = 0.521. \tag{73}$$

Consequently, the separation is moving upstream in the vortex frame (from right to left) at the instant of the boundary-layer eruption; note that the terminology 'upstream' is used here to imply a direction opposite to the local mainstream velocity. It should be noted that the wall is moving in the vortex frame and this does present a difficulty in classifying the separation; however, it appears that the relevant criterion here is the motion of the separation relative to the local external mainstream direction. Thus, this situation may also be thought of as corresponding to what Van Dommelen (1981) has referred to as 'upstream-slipping separation'.

6. Calculated results

The nature of the flow evolution may be understood through examination of the instantaneous streamline patterns as time progresses as well as the behaviour of the displacement thickness. These quantities are relatively easy to evaluate from the results of an Eulerian computation but require some additional effort to extract from Lagrangian data. First it is necessary to evaluate the y particle positions. In accordance with (26), define a transformed variable $\hat{y}$ on the finite range $(0, 1)$ by

$$\hat{y} = \frac{2}{\pi}\arctan y. \tag{74}$$

In terms of this variable, the continuity equation (17) becomes

$$\frac{\partial \hat{x}}{\partial \hat{\xi}}\frac{\partial \hat{y}}{\partial \hat{\eta}} - \frac{\partial \hat{x}}{\partial \hat{\eta}}\frac{\partial \hat{y}}{\partial \hat{\xi}} = \frac{U_e(\hat{x})\,Z(\hat{y})}{U_e(\hat{\xi})\,Z(\hat{\eta})}, \tag{75}$$

where U_e and Z are defined in (25) and (36) respectively. If at any time t, $\hat{x}(\hat{\xi}, \hat{\eta}, t)$ is known from a solution of (27) and (28), it is evident that (75) is a first-order equation for $\hat{y}$. The characteristic curves are $\hat{x}$ = constant and the subsidiary equations are of the form

$$\frac{\mathrm{d}\hat{\xi}}{A} = \frac{\mathrm{d}\hat{\eta}}{B} = \frac{\mathrm{d}\hat{y}}{C} = \mathrm{d}\hat{s}, \tag{76}$$

where

$$A = -\frac{\partial \hat{x}}{\partial \hat{\eta}}, \quad B = \frac{\partial \hat{x}}{\partial \hat{\xi}}, \quad C = \frac{U_e(\hat{x})\,Z(\hat{y})}{U_e(\hat{\xi})\,Z(\hat{\eta})}, \tag{77}$$

and $\hat{s}$ is a parameter along the characteristic $\hat{x}$ = constant. Generally, the integration of (76) is initiated at some selected value of $\hat{\xi}$ on the wall where $\hat{y} = 0$. On the wall

$$x = \xi - (t - t_0), \tag{78}$$

which from (23) and (24) fixes $\hat{x}$ for a specific choice of $\hat{\xi}$ at time t. The integration of (76) was accomplished using a second-order predictor-corrector method (Peridier & Walker 1989). This integration generates a sequence of points $(\hat{\xi}^k, \hat{\eta}^k)$ and corresponding values $\hat{y}^k$ which define a specific contour $\hat{x}$ = constant. If A^k and B^k denote the coefficients in (77) evaluated at the kth point on the contour, the step size in $\hat{s}$ was selected so that

$$\Delta\hat{s} = \frac{\Delta\hat{\xi}}{[(A^k)^2 + (B^k)^2]^{\frac{1}{2}}}. \tag{79}$$

This criterion restricts the step along the curve $\hat{x}$ = constant to a mesh length in $\hat{\xi}$ and was judged to be small enough to ensure an accurate evaluation of $\hat{y}$.

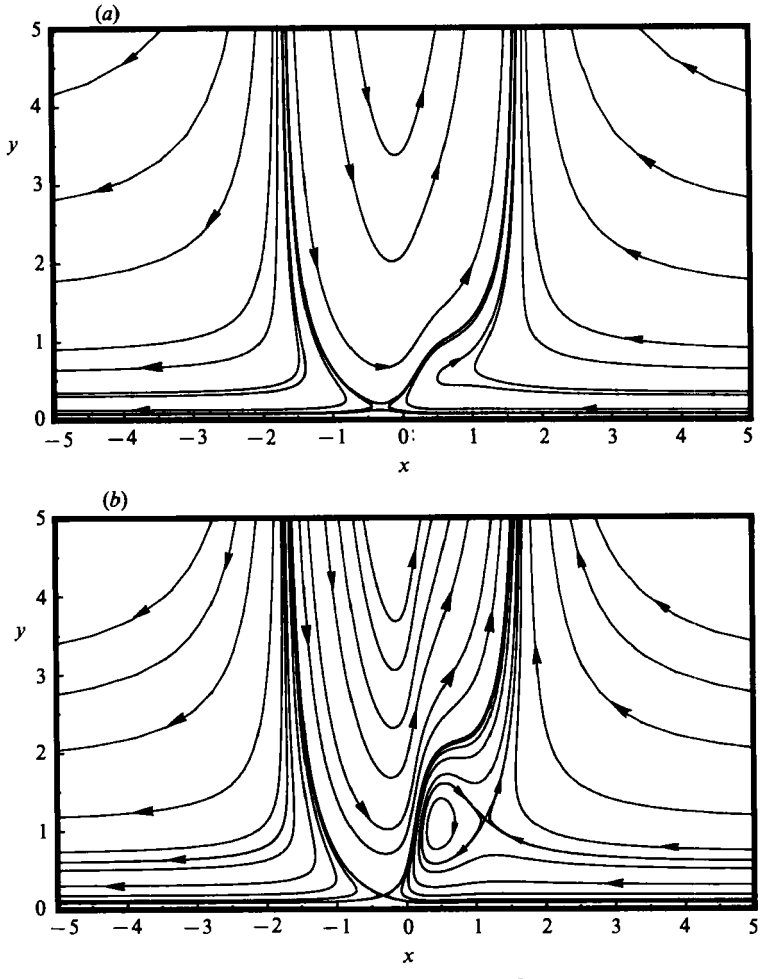

FIGURE 3(a, b). For caption see facing page.

A stream function Ψ may be defined in terms of the velocity u in the vortex frame, as well as a subsidiary stream function $\tilde{\psi}$ in terms of U, by

$$u = \frac{\partial \Psi}{\partial y}, \quad U = \frac{\partial \tilde{\psi}}{\partial y}, \tag{80}$$

and it follows from (21) that

$$\Psi = U_e(x)\tilde{\psi}(x, y, t) - y. \tag{81}$$

In terms of the transformed coordinate (74)

$$\tilde{\psi} = \int_0^{\hat{y}} U(\hat{\xi}, \hat{\eta}, t)\Big|_{\hat{x}=\text{const}} \frac{\mathrm{d}\alpha}{Z(\alpha)}, \tag{82}$$

and $\tilde{\psi}$ and Ψ were evaluated as follows. As the integration of (75) proceeds up a particular characteristic $\hat{x} =$ constant, values of $\hat{y}$ were obtained at a sequence of points along the characteristic; values of $\tilde{\psi}$ were obtained along this same characteristic by integrating (82) in a step-by-step manner using a procedure based on the trapezoidal rule. At each point along the characteristic, values of y (from (74))

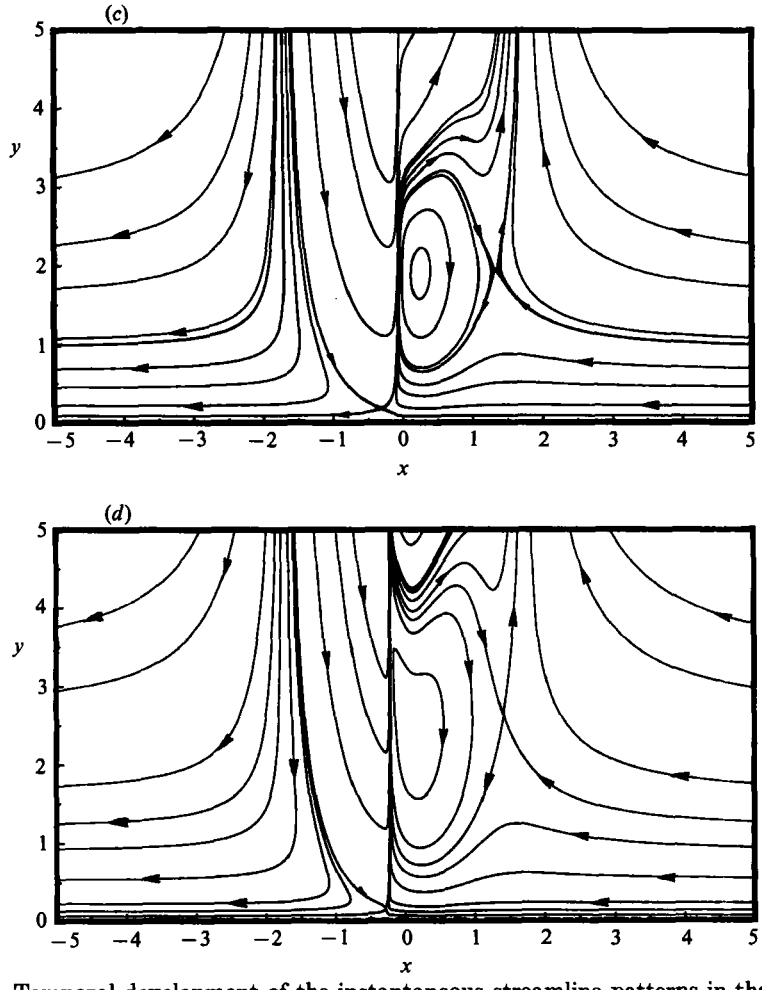

FIGURE 3. Temporal development of the instantaneous streamline patterns in the vortex frame. (*a*) $t = 0.25$; (*b*) $t = 0.45$; (*c*) $t = 0.75$; (*d*) $t = t_s = 0.989$.

and $\tilde{\psi}$ may be used to yield values of Ψ in (81). By performing this same type of calculation along a number of characteristics, values of Ψ were defined throughout a mesh in the (x, y)-plane and evaluation of contours of constant Ψ produces the instantaneous streamlines.

The flow patterns at $t = 0.25$ are shown in figure 3(*a*) in a frame of reference convecting with the vortex, in terms of the physical coordinate x and boundary-layer coordinate y. At this stage the flow pattern is almost symmetrical consisting of: (i) motion from upstream infinity upward and toward an outflow stagnation point in the mainstream at $x = \sqrt{3}$; (ii) motion downward and away from an inflow stagnation point at $x = -\sqrt{3}$ and (iii) an inflow, then outflow underneath the vortex itself. In the vortex frame the wall moves to the left with a speed of unity and there is a single stagnation point near $x = -0.3$ just above the wall. A recirculating eddy appears in the streamline patterns at $t = 0.281$ (Walker 1978) and may be observed at a later stage of development in figure 3(*b*) at $t = 0.45$. The eddy thickens rapidly in the streamwise direction and then starts to grow in a direction normal to the wall as may be seen in figure 3(*c*) at $t = 0.75$. The streamlines on the left side of the eddy

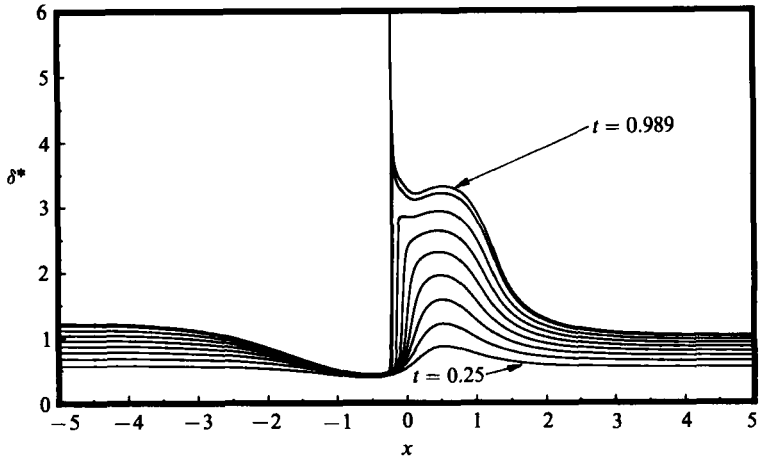

FIGURE 4. Temporal development of the displacement thickness; plotted curves are at $t = 0.25$ (0.10) 0.95 and $t_s = 0.989$.

run very close there and this is an indication of an intense variation in the flow field which is developing locally. From a physical standpoint, the eddy gives rise to a blocking effect as the boundary-layer fluid, under the action of the pressure gradient, is deflected upward and forced to climb over an expanding zone of recirculation. This effect gives rise to increasing normal velocities near the left side of the eddy and the progressive formation of what appears to be a developing shear layer. The streamlines at $t = t_s = 0.989$ are shown in figure 3(*d*) where a continuation of the aforementioned trends should be noted. In the interval from 0.45 to 0.989, the eddy has doubled in width but is almost four times larger in the vertical direction; the eddy centre has also progressively moved away from the surface. One new feature in figure 3(*d*) is that the streamlines at the top of the eddy have developed a 'spike' and the recirculation zone is apparently being drawn into a zone of intense variation near $x_s = -0.218$.

The character of the boundary-layer growth may be illustrated through the displacement thickness, defined in terms of the velocity in the laboratory frame of reference by

$$\delta^*(x,t) = \int_0^\infty \left\{1 - \frac{u+1}{U_e(x)}\right\} \mathrm{d}y, \tag{83}$$

and it follows from (21) that

$$\delta^* = \int_0^\infty \left\{1 - U(\hat{\xi},\hat{\eta},t)\right\}\Big|_{\hat{x}} \mathrm{d}y, \tag{84}$$

or equivalently from (80)

$$\delta^* = \lim_{y\to\infty}\{y - \tilde{\psi}\} = \lim_{\hat{y}\to 1}\{\tan(\tfrac{1}{2}\pi\hat{y}) - \tilde{\psi}\}. \tag{85}$$

Thus, for a specific value of $\hat{x}$, δ^* was evaluated by computing the integral in (84) as the integration proceeded up the characteristic. The temporal development of δ^* is shown in figure 4 in the vortex frame, where it may be seen that explosive boundary-layer growth finally occurs near $x_s = -0.214$. The rather abrupt nature of the phenomena should be noted. Until around $t = 0.85$ the growing recirculating eddy

has caused significant but unremarkable thickening of the boundary layer over a streamwise extent $O(1)$. However, in the interval between $t = 0.85$ and 0.989, the boundary-layer flow abruptly focuses into a band which is very narrow in the streamwise direction; the maximum displacement thickness increases substantially during the interval and, on a scale where $x = O(1)$, the local displacement surface appears as a sharp spike. As illustrated in figure 4, the phenomena develops and takes place in a frame of reference moving with the vortex; an observer in this frame would see a very localized zone of relatively abrupt boundary-layer growth which appears to be moving upstream in its final stages.

One point should be noted in connection with the calculation of δ^*. In the early stages of the motion, the displacement-thickness distribution is relatively smooth and can be defined by computing δ^* along a number of characteristics corresponding to the number of subdivisions in the $\hat{\xi}$-mesh. However, an integration along a characteristic may be started at any location on the $\hat{\xi}$-axis and, in the latter stages of the integration when δ^* develops a spike, it was necessary to compute many additional characteristic contours. This was carried out using a systematic resolution-enhancement procedure near the contour $\hat{x} = \hat{x}_s$ in order to accurately represent δ^* in figure 4 as well as to locate the 'tip' of the spike.

7. The terminal structure

Once a stationary point occurs in $x(\xi, \eta, t)$, a singularity has developed in the solution of the boundary-layer equations. Van Dommelen (1981) and Elliott *et al.* (1983) have investigated the structure of a class of possible singularities and what follows is a description of their results in terms of Eulerian coordinates. As a boundary layer proceeds toward an eruptive interaction of the type depicted in figure 4, the layer bifurcates locally near x_s into three zones which are shown schematically in figure 5(*a*). It should be noted that in the numerical integrations, the entire zone depicted in figure 5(*a*) appears for the most part as a spike on a scale where $x - x_s$ is $O(1)$. Thus, the schematic in figure 5(*a*) should be interpreted as having a considerably expanded scale in the x-direction in order to show the internal structure of the erupting 'spike' depicted in figure 4. The local dynamics are driven by a central region II sandwiched between two passive layers, one near the wall (region I) and one which moves rapidly away from the wall (region III). The terminal solution in zone II is a function of the scaled variables

$$\tilde{X} = \frac{x - x_s - K(t_s - t)}{(t_s - t)^{\frac{3}{2}}}, \quad \tilde{Y} = (t_s - t)^{\frac{1}{2}} y, \tag{86}$$

where y is the conventional boundary-layer variable (scaled with respect to $Re^{\frac{1}{8}}$ as in (1)). The variable $\tilde{X}$ measures streamwise distance in a coordinate system which is moving upstream with speed K (for $K > 0$) and whose origin arrives at x_s at time $t = t_s$; in physical space this region thins proportional to $(t_s - t)^{\frac{3}{2}}$ as $t \to t_s^-$. The variable $\tilde{Y}$ measures normal distance from the wall in a region which is thickening explosively like $(t_s - t)^{-\frac{1}{4}}$. Within zone II, the streamwise velocity is given by

$$u = -K + (t_s - t)^{\frac{1}{2}} \tilde{U}(\tilde{X}, \tilde{Y}) + \ldots \tag{87}$$

and consequently zone II is a vorticity-depleted region which is moving upstream (for upstream-slipping separation, $K > 0$) and where the flow is almost uniform. A solution for $\tilde{U}$ may be obtained and details are given by Elliott *et al.* (1983). However, it should be noted that the equation governing $\tilde{U}$ is nonlinear and inviscid; the

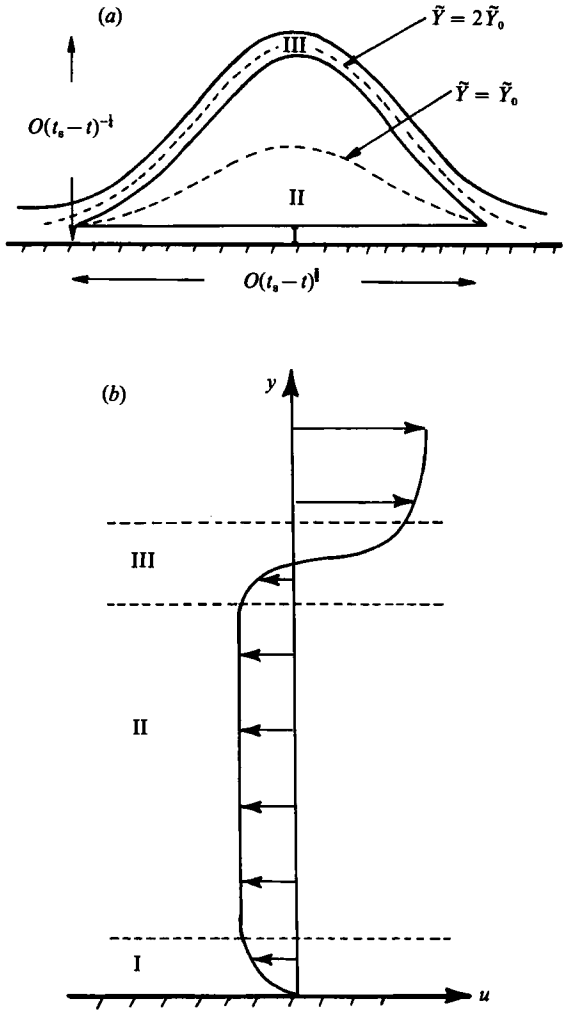

FIGURE 5. Schematic of boundary-layer structure near a point of eruption. (*a*) Structure near x_s (not to scale); (*b*) a typical velocity profile near $x = x_s$ (for a stationary wall).

solution is symmetric about a curve $\tilde{Y} = \tilde{Y}_0(\tilde{X})$ which can be found analytically and which bisects region II as indicated in figure 5(*a*). The curve $\tilde{Y} = 2\tilde{Y}_0(\tilde{X})$ thus defines the top of region II. The velocity function $\tilde{U}$ has a minimum at $\tilde{Y} = \tilde{Y}_0$ at each $\tilde{X}$-station but increases to become large and positive at the top and bottom of region II; in fact

$$\tilde{U} \sim \frac{4}{\tilde{Y}^2} \quad \text{as} \quad \tilde{Y} \to 0, \tag{88}$$

$$\tilde{U} \sim \frac{4}{(\tilde{Y} - 2\tilde{Y}_0)^2} \quad \text{as} \quad \tilde{Y} \to 2\tilde{Y}_0(\tilde{X}). \tag{89}$$

Note that in view of (88) and (89), the streamwise velocity in (87) starts to deviate progressively from $-K$ as zones I and III are approached for fixed $t_s - t$. In general, the velocity is reduced to relative rest on the wall in zone I and is adjusted across the shear layer III to meet the positive mainstream velocity in the upper portion of the

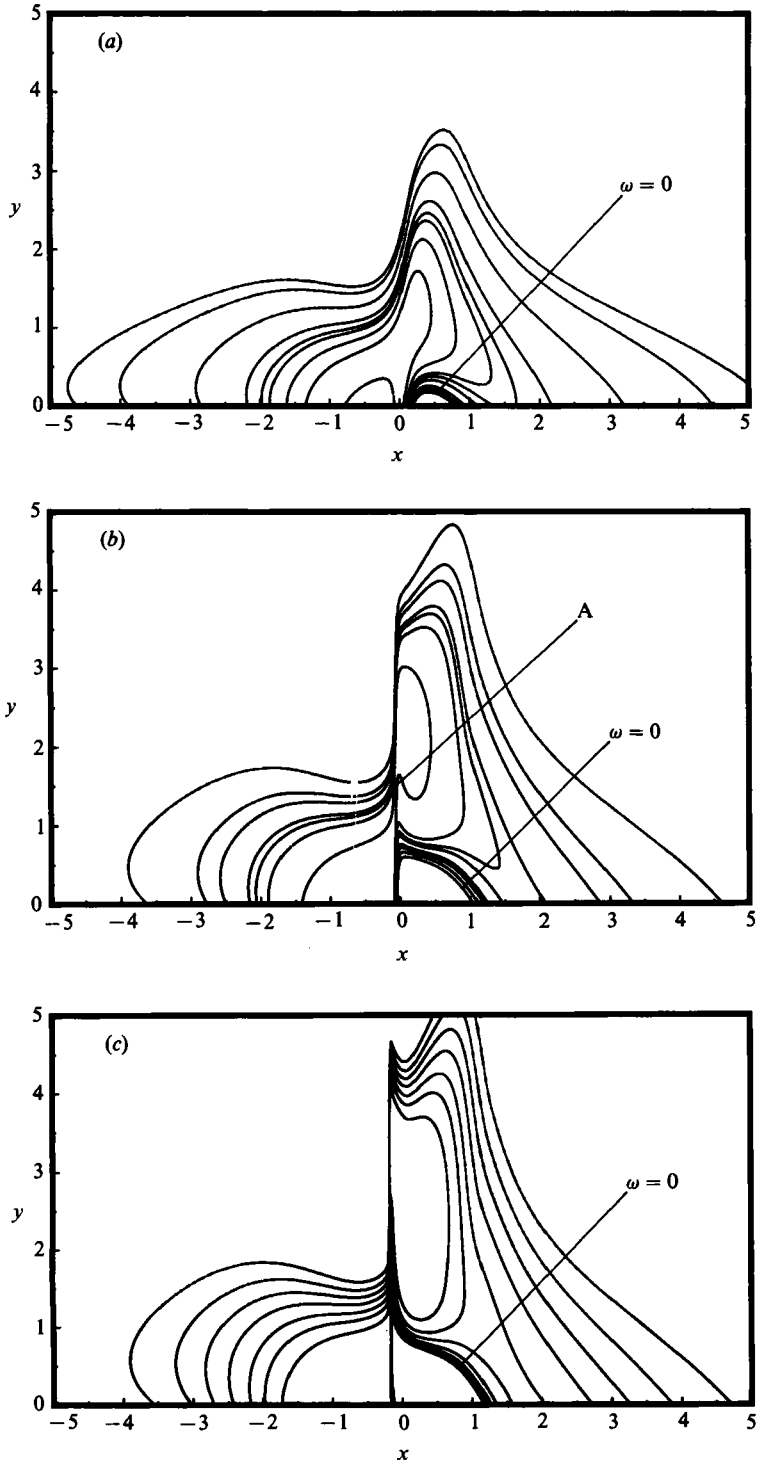

FIGURE 6. Evolution of the constant-vorticity contours. (*a*) $t = 0.45$; (*b*) $t = 0.75$; (*c*) $t = 0.95$.

boundary layer. A typical profile shape expected within the erupting spike is shown schematically in figure 5(*b*) for a stationary wall. It an be shown (Elliott *et al.* 1983) that

$$U = O(\tilde{X}^{\frac{1}{3}}) \quad \text{as} \quad |\tilde{X}| \to \infty, \tag{90}$$

and thus it may be inferred from (86) and (87) that u deviates progressively from $-K$ at the streamwise extremities of the region depicted in figure 5(*a*) in order to meet the conventional boundary layer to either side.

An important aspect of the terminal singular structure described by Van Dommelen (1981) and Elliott *et al.* (1983) is that by the stage that an eruptive spike starts to develop, the local boundary-layer flow 'forgets' the specific external pressure gradient which initiated the separation process; that is, the equation governing $\tilde{U}$ in the central zone II is independent of the mainstream pressure gradient. Consequently, the terminal structure appears to be a generic end state for all two-dimensional unsteady boundary layers that ultimately interact strongly with the mainstream, at least for the apparently common situation of 'upstream-slipping separation'. Van Dommelen & Shen (1982) have shown that the terminal state is realized in the case of the impulsively started circular cylinder and here it will be shown that the same state is reached in the present situation.

It is worthwhile tracking the development of the equi-vorticity lines; ω is readily evaluated from Lagrangian data using (67) and contours of constant ω are shown in figure 6 at $t = 0.45, 0.75$ and 0.95. In figure 6(*a*) at $t = 0.45$, it may be seen that a zero-vorticity line is present which touches the wall at about $x = 0.25$ and $x = 0.75$; this line first appears with the onset of the recirculating eddy at $t = 0.281$. Between the wall and the zero-vorticity line, ω is positive; elsewhere ω is negative and actual magnitudes may be inferred from a plot of the wall shear (that will be shown in figure 8), since all equi-vorticity lines begin and end on the wall. The maximum magnitude of vorticity in figure 6(*a*), for example, occurs in the contour near $x = -0.5$ closest to the wall; the contours to either side have progressively smaller values of ω. In figure 6(*b*) at $t = 0.75$, it may be seen that the constant-ω contours have deformed to start to form an inverted 'V' near $x = 0$ in the location labelled A. By $t = 0.95$, it may be seen in figure 6(*c*) that most of the contours above $x = -0.214$ have developed this inverted V pattern which is now considerably stretched in the vertical direction. This development is consistent with the terminal structure sketched in figure 5(*a*); the two sides of the inverted V, where the equi-vorticity lines are congregating, form the moving shear layer denoted as region III in figure 5(*a*). Note that the erupting spike in figure 6(*c*) appears to act as a sink, dragging the surrounding equi-vorticity lines into it. The region underneath the V is too narrow to be seen on the scale of figure 6(*c*) but is the vorticity-depleted zone labelled region II in figure 5(*a*).

In figure 7 the velocity profiles near x_s are plotted just before $t = t_s$ across the boundary layer and these confirm the terminal structure shown schematically in figure 5(*a*). At $x = x_s$ the major part of the profile is almost flat and the boundary layer is very thick locally. A shear layer is present near the wall and in the upper part of the boundary layer to adjust the velocity from the uniform value of $-K$. Note that in this case the wall is moving to the left and so the adjustment in the lower shear layer takes place from $-K$ to -1, as opposed to the schematic in figure 5(*b*), which pertains to a fixed wall, and where the adjustment is from $-K$ to 0. It should be noted that, though hardly visible in figure 7, there is a local maximum clearly exhibited in the numerical results for the velocity profile relatively near the wall, in addition to the minimum that is evident further out. It is believed that this maximum probably lies within the $O(1)$ wall layer (region I in figure 5*a*),

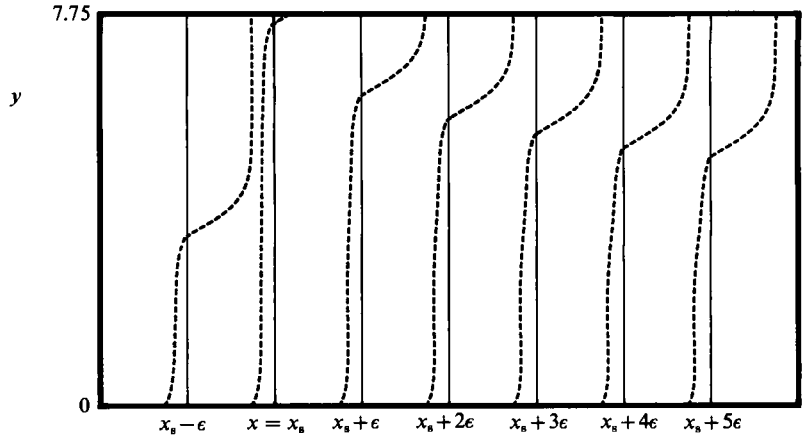

FIGURE 7. Velocity profiles near $x = x_s$ just before t_s; here $\epsilon = 1.05 \times 10^{-3}$.

asymptotically, in keeping with the behaviour indicated in (87) and (88), rather than occurring within the thick intermediate layer (region II in figure 5*a*). At the same time, however, it is worthwhile to mention that the assumptions made by Elliott *et al.* (1983) concerning the symmetry of region II (cf. figure 5*a*) can be relaxed to accommodate the possible occurrence of local maxima within region II. The location $x = x_s$ corresponds to the streamwise location of the spike depicted in figure 4. To the left and right of x_s, it may be noted that a significant portion of the profiles are also flat but that the upper shear layer is returning toward the wall.

The theory of Van Dommelen & Shen (1980) and Elliott *et al.* (1983) predicts that the maximum value of the displacement thickness is of the form

$$\delta^*_{\max} = \frac{C}{(t_s - t)^m}, \tag{91}$$

where $m = \frac{1}{4}$. Owing to the nature of the local displacement thickness near the spike, it is difficult to compute a value of $\delta^*_{\max}$ near $t = t_s$ with a high degree of accuracy. Nevertheless, a least-squares curve fit of (91) to the computed results for $\delta^*_{\max}$ in the time interval $0.900 < t < 0.986$ produced the following values:

$$C = 1.71 \pm 0.02, \quad m = 0.253 \pm 0.003. \tag{92}$$

This value of m closely confirms that growth rate of the boundary layer near $t = t_s$ predicted by Elliott *et al.* (1983).

Lastly consider the behaviour of the wall shear defined by

$$\tau_w(x, t) = \left.\frac{\partial u}{\partial y}\right|_{y=0}, \tag{93}$$

and in Lagrangian coordinates by using

$$\tau_w(x, t) = U_e(x) \left.\frac{\partial u}{\partial \eta}\right|_{\eta=0}. \tag{94}$$

The gradient in (94) was evaluated with a four-point sloping difference and the development is shown in figure 8. It may be observed that during the course of the integration, the wall shear remains smooth and regular; this is expected since the

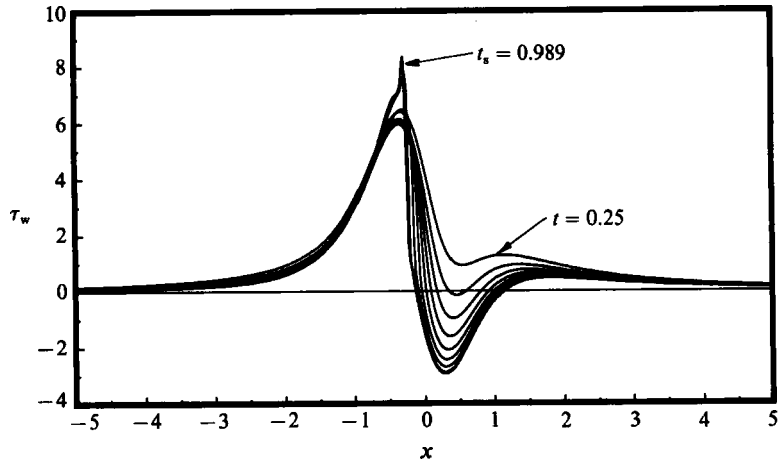

FIGURE 8. Temporal development of the wall shear; the distributions are plotted for $t = 0.25$ (0.10) 0.95 and at $t_s = 0.989$.

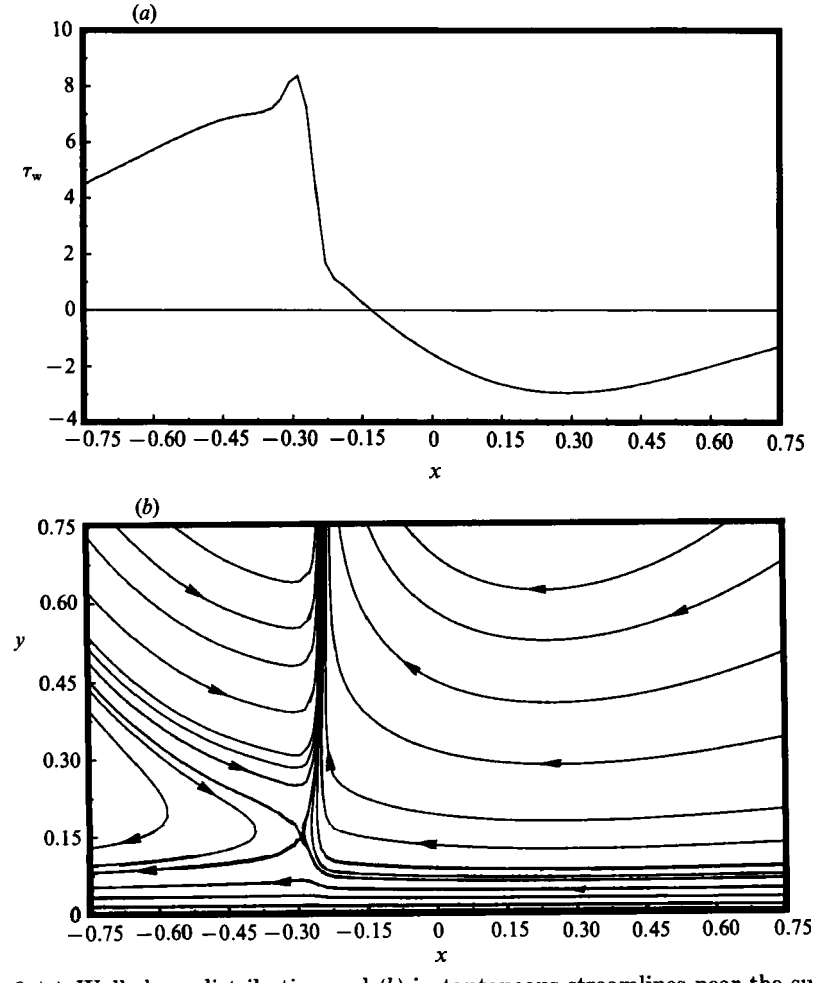

FIGURE 9. (a) Wall shear distribution and (b) instantaneous streamlines near the surface on an expanded streamwise scale at t_s.

solution in zone I (cf figure 5*a*) is a function of y alone (Elliott *et al.* 1983). One feature in figure 8 is worthy of note near $x = -0.30$ where the wall shear rises abruptly as $t \to t_s$; this occurs to the left of where the singularity develops at $x_s = -0.214$ and was observed to form for all three sets of mesh sizes. To examine a possible cause for this behaviour, the wall shear and instantaneous streamlines are plotted on an expanded scale in figure 9(*a*, *b*). Note that no attempt has been made in these graphs (as well as the previous plots) to smooth the results and the plotter has simply connected values at each mesh point. On the scale of figure 9(*a*), the distribution of τ_w appears well-behaved. The maximum in wall shear (corresponding to the tip of the 'spike' in figure 8) coincides with the streamwise location of the stagnation point near $x = -0.30$ and close to the surface in figure 9(*b*). With the evolution of large updraughts near the singularity at $x_s = -0.214$, the stagnation point is lifted somewhat from the wall giving rise to a pinching of the streamlines and a mildly intense variation in τ_w near $t = t_s$.

8. Discussion

It has been demonstrated that the vortex-driven unsteady boundary layer considered here for the limit problem $Re \to \infty$ develops a singularity on the zero-vorticity line. Furthermore, the terminal singularity structure is identical to that reached for the impulsively started circular cylinder by Van Dommelen & Shen (1980, 1982) and described by Elliott, *et al.* (1983). In the terminal stage of the boundary-layer development the flow focuses rapidly into a narrow eruptive spike that grows explosively away from the surface. For the limit problem $Re \to \infty$, the eruption appears to take place at a point on a scale where x is $O(1)$.

Elliott *et al.* (1983) have discussed the next stage in the eruptive process wherein interaction with the external flow comes into play when $t_s - t$ is $O(Re^{-\frac{8}{11}})$. This interaction occurs over a streamwise lengthscale where $x - x_s$ is $O(Re^{-\frac{3}{11}})$. The normal dimension of the intermediate zone II in figure 5(*a*) grows to become $O(Re^{-\frac{5}{11}})$ while shear layers I and III remain $O(Re^{-\frac{1}{2}})$. The pressure distribution which governs the subsequent development in zone II is determined through evaluation of a Cauchy integral involving the displacement thickness distribution due to the rapidly thickening central zone. This phase of the flow development will be referred to here as the 'first interactive stage' and was originally formulated by Elliott *et al.* (1983). However, because of the complex nature of this interaction problem, as well as the challenging type of boundary conditions (which are similar to (88) and (89)), no numerical solutions of the first interactive stage have yet been produced. It may be expected that this stage will also terminate in a singularity, and that in a limit analysis $Re \to \infty$ it will be necessary to compute a whole series of intermediate stages before the erupting vorticity from near the surface penetrates an $O(1)$ distance from the wall.

One attractive feature of the model problem is that the general nature of the viscous–inviscid interaction has been documented by experiment (Harvey & Perry 1971; Walker *et al.* 1987; Chu & Falco 1988). The net result is that a secondary vortex is ejected from the boundary layer and the secondary vortex is generally of comparable strength and dimension to the original primary vortex. The precise details of how this takes place are not entirely understood. It is evident from figure 3(*d*) that, by t_s, the recirculating eddy is being lifted off the wall and also drawn into the eruptive spike. It is possible that the next stage in the process consists of compression of the eddy which is then sucked into the erupting spike and

subsequently thrown out into the external flow. Flow visualization (Walker *et al.* 1987) suggests this scenario but further theoretical work is required to confirm this physical picture of how the secondary vortex reaches the external region. Clearly a description of the complete problem of breakaway of the boundary layer into the mainstream for the limit problem $Re \to \infty$ is rather complex. An alternative approach to consider the nature of the eruption is interacting boundary-layer (IBL) theory in which a finite but large value of Re is assumed; in this approach the thickening boundary layer influences the external flow and the mainstream pressure gradient changes with time, as opposed to the limit problem where $\mathrm{d}p_\infty/\mathrm{d}x$ is prescribed. Experience with steady interacting boundary-layer methods hints that such schemes may relieve the singularity encountered in the limit problem and permit the computations to proceed much further in time. The recent work of Henkes & Veldman (1987), Chuang & Conlisk (1989) and Riley & Vasantha (1990) on the impulsively started circular cylinder and problems in vortex-induced separation suggests that interacting boundary-layer methods may in some sense mitigate the unsteady separation singularity. By contrast, however, in part 2 (Peridier *et al.* 1991), IBL calculations are carried out for the present problem and it is shown fairly conclusively that the approach also breaks down in finite time in *advance* of the breakdown time t_s for the limit problem. The new singularity associated with the breakdown of the IBL formulation is found to be that described by Smith (1988); see also Hoyle, Smith & Walker (1991).

It is evident that the Lagrangian method is very effective at accurately tracing the boundary-layer solution all the way to the evolution of the separation singularity. At present it is the only scheme in which the integrations can be continued this far. Although conventional Eulerian methods which employ a fixed spatial mesh are clearly not suited to the calculation of such eruptive phenomena, an Eulerian approach may well be feasible if a time-dependent adaptive mesh scheme is developed wherein local refinement of the mesh is carried out dynamically as soon as strong updraughts start to occur. The present factored ADI method with upwind-downwind differencing is a robust numerical algorithm particularly suited to this type of problem. However it should be noted that careful checking of the results during the course of the integration may be necessary in other applications of the approach. In the present problem, stability problems were encountered near the stagnation point close to the wall (see, for example, figure 3*a*) which could only be inhibited by reduced time steps.

Lastly, it is of interest to comment on the relevance of the phenomenon described in this study to the processes of regeneration of new vorticity at the surface in transitional and fully turbulent boundary layers. In both environments, the basic element of the flow structure appears to be the convected hairpin vortex (Walker 1990*b*; Smith *et al.* 1990, 1991). Such vortices expose the surface flow to a moving zone of adverse pressure gradient and are observed to eventually actuate eruptions of the viscous flow near the surface. Although the details of the process are more complex in three-dimensional flows (Van Dommelen & Cowley 1990), the basic character of the eruptive process is the same as discussed in this paper. The event develops in a frame of reference moving with the vortex, and the induced adverse pressure gradient ultimately provokes an abrupt and tightly focused narrow-band eruption. It is evident from the present results that the erupting 'spike' will contain elevated levels of vorticity which is subsequently observed to roll over into a new secondary hairpin vortex (Smith *et al.* 1990, 1991). End-view visualization in both transitional and fully turbulent boundary layers (Smith *et al.* 1991) suggests that

breakdown of the surface layers takes place intermittently and predominantly in this manner, with narrow 'spikes' of erupting fluid which penetrate into the outer regions of the boundary layer.

This work was supported by Air Force Office of Scientific Research under grant AFOSR-89-0065 and AFOSR-89-0475 as well as a NATO travel grant 86/197. The referees' comments are gratefully acknowledged.

Appendix

In this Appendix the finite-difference operator notation utilized in this discussion is explicitly defined for completeness. Here $(\hat{\xi}, \hat{\eta})$ are independent spatial coordinates and the uniform mesh spacing in each direction is $(\Delta\hat{\xi}, \Delta\hat{\eta})$ respectively. The general form of the enlargement operators in the $\hat{\xi}$- and $\hat{\eta}$-directions are defined by

$$\mathrm{E}^p_{\hat{\xi}}\, u(\hat{\xi}, \hat{\eta}) = u(\hat{\xi} + p\,\Delta\hat{\xi}, \hat{\eta}), \tag{A 1}$$

$$\mathrm{E}^p_{\hat{\eta}}\, u(\hat{\xi}, \hat{\eta}) = u(\hat{\xi}, \hat{\eta} + p\,\Delta\hat{\eta}), \tag{A 2}$$

where p is an arbitrary constant. The enlargement operator simply shifts the argument of the function. The central-difference operators $\delta_{\hat{\xi}}$ and $\delta_{\hat{\eta}}$ are defined by (49) and consequently expressions such as

$$\delta_{\hat{\xi}} u(\hat{\xi}, \hat{\eta}) = u(\hat{\xi} + \tfrac{1}{2}\Delta\hat{\xi}, \hat{\eta}) - u(\hat{\xi} - \tfrac{1}{2}\Delta\hat{\xi}, \hat{\eta}), \tag{A 3}$$

$$\delta_{\hat{\eta}} u(\hat{\xi}, \hat{\eta}) = u(\hat{\xi}, \hat{\eta} + \tfrac{1}{2}\Delta\hat{\eta}) - u(\hat{\xi}, \hat{\eta} - \tfrac{1}{2}\Delta\hat{\eta}), \tag{A 4}$$

correspond to the central difference of a function with one spatial variable held fixed. Finally, the averaging operators $\mu_{\hat{\xi}}$ and $\mu_{\hat{\eta}}$ are defined by (55) and therefore

$$\mu_{\hat{\xi}} u(\hat{\xi}, \hat{\eta}) = \tfrac{1}{2}(u(\hat{\xi} + \tfrac{1}{2}\Delta\hat{\xi}, \hat{\eta}) + u(\hat{\xi} - \tfrac{1}{2}\Delta\hat{\xi}, \hat{\eta})), \tag{A 5}$$

$$\mu_{\hat{\eta}} u(\hat{\xi}, \hat{\eta}) = \tfrac{1}{2}(u(\hat{\xi}, \hat{\eta} + \tfrac{1}{2}\Delta\hat{\eta}) + u(\hat{\xi}, \hat{\eta} - \tfrac{1}{2}\Delta\hat{\eta})), \tag{A 6}$$

correspond to function averages with one spatial variable held fixed.

REFERENCES

Acarlar, M. S. & Smith, C. R. 1987*a* A study of hairpin vortices in a laminar boundary layer. Part 1. Hairpin vortices generated by hemisphere protuberances. *J. Fluid Mech.* **175**, 1–41.

Acarlar, M. S. & Smith, C. R. 1987*b* A study of hairpin vortices in a laminar boundary layer. Part 2. Hairpin vortices generated by fluid injection. *J. Fluid Mech.* **175**, 43–83.

Beam, R. M. & Warming, R. F. 1978 An implicit factored scheme for the compressible Navier–Stokes equations. *AIAA J.* **16**, 393–402.

Cebeci, T. 1986 Unsteady boundary layers with an intelligent numerical scheme. *J. Fluid Mech.* **163**, 129–140.

Chu, C. C. & Falco, R. E. 1988 Vortex ring/viscous wall layer interaction model of the turbulence production process near walls. *Exp. Fluids.* **6**, 305.

Chuang, F. S. & Conlisk, A. T. 1989 Effect of interaction on the boundary layer induced by a convected rectilinear vortex. *J. Fluid Mech.* **200**, 337–365.

Collins, W. M. & Dennis, S. C. R. 1973 Flow past an impulsively started circular cylinder. *J. Fluid Mech.* **60**, 105–127.

Conlisk, A. T. 1989 The pressure field in intense vortex-boundary layer interaction. *27th Aerospace Sciences Meeting, Reno, NV, AIAA Paper.* 89–0293.

Cousteix, J. 1986 Three-dimensional and unsteady boundary-layer computations, *Ann. Rev. Fluid Mech.* **18**, 173–196.

COWLEY, S. J. 1983 Computer extension and analytic continuation of Blasius' expansion for impulsive flow past a circular cylinder. *J. Fluid Mech.* **135**, 389–405.

COWLEY, S. J., VAN DOMMELEN, L. L. & LAM, S. T. 1990 On the use of Lagrangian variables in descriptions of unsteady boundary-layer separation. *Phil. Trans. R. Soc. Lond.* **A333**, 343–378.

DOLIGALSKI, T. L. & WALKER, J. D. A. 1978 Shear layer breakdown due to vortex motion. In *Coherent Structure of Turbulent Boundary Layers* (ed. C. R. Smith & D. E.Abbott), pp. 288–332. AFOSR/Lehigh University Workshop.

DOLIGALSKI, T. L. & WALKER, J. D. A. 1984 The boundary layer induced by a convected two-dimensional vortex. *J. Fluid Mech.* **139**, 1–28.

ECE, M. C., WALKER, J. D. A. & DOLIGALSKI, T. L. 1984 The boundary layer on an impulsively started rotating and translating cylinder. *Phys. Fluids* **23**, 1077–1089.

ELLIOTT, J. W., COWLEY, S. J. & SMITH, F. T. 1983 Breakdown of boundary layers: (i) on moving surfaces; (ii) in self-similar unsteady flow; (iii) in fully unsteady flow. *Geophy. Astrophys. Fluid Dyn.* **25**, 77–138.

ELLIOTT, J. W. & SMITH, F. T. 1987 Dynamic stall due to unsteady marginal separation. *J. Fluid Mech.* **179**, 489–512.

ERSOY, S. & WALKER, J. D. A. 1985 Viscous flow induced by counterrotating vortices. *Phys. Fluids* **28**, 2687–2698.

ERSOY, S. & WALKER, J. D. A. 1986 Flow induced at a wall by a vortex pair. *AIAA J.* **24**, 1597–1605.

GOLDSTEIN, S. 1948 On laminar boundary-layer flow near a point of separation. *Q. J. Mech. App. Maths* **1**, 43–69.

HARVEY, J. K. & PERRY, F. J. 1971 Flowfield produced by trailing vortices in the vicinity of the ground. *AIAA J.* **9**, 1659–1660.

HEAD, M. R. & BANDYOPADHYAY, P. 1981 New aspects of turbulent boundary layer structure. *J. Fluid Mech.* **107**, 297–338.

HENKES, R. A. W. M. & VELDMAN, A. E. P. 1987 On the breakdown of the steady and unsteady interacting boundary-layer description. *J. Fluid Mech.* **179**, 513–529.

HOYLE, J. M., SMITH F. T. & WALKER, J. D. A. 1991 On sublayer eruption and vortex formation. *Comput. Phys. Commun.* **65**, 151–157.

LAM, S. T. 1988 On high-Reynolds-number-laminar flows through a curved pipe, and past a rotating cylinder. Ph.D. thesis, University of London.

MCCROSKEY, W. J. 1982 Unsteady Airfoils. *Ann. Rev. Fluid Mech.* **14**, 285–311.

MOORE, F. K. 1958 On the separation of the unsteady boundary layer. In *Boundary Layer Research* (ed.H. G. Görtler), pp. 296–311. Springer.

PERIDIER, V. J., SMITH, F. T. & WALKER, J. D. A. 1988 Methods for the calculation of unsteady separation. *AIAA Paper* 88–0604.

PERIDIER, V. J., SMITH, F. T. & WALKER, J. D. A. 1991 Vortex-induced boundary–layer separation. Part 2. Unsteady interacting boundary-layer theory. *J. Fluid Mech.* **232**, 133–165.

PERIDIER, V. J. & WALKER, J. D. A. 1988 An algorithm for unsteady flows with strong convection. *NASA Tech. Mem.* 100828; ICOMP–88–5, NASA Lewis Research Center.

PERIDIER, V. J. & WALKER, J. D. A. 1989 Vortex-induced boundary-layer separation, Rep. FM-13. Dept. of Mechanical Engineering and Mechanics, Lehigh University; AFOSR-TR-90-0458 (available as ADA-221564).

PROUDMAN, I. & JOHNSON, K. 1962 Boundary-layer growth near a rear stagnation point. *J. Fluid Mech.* **12**, 161–168.

RILEY, N. 1975 Unsteady laminar boundary layers. *SIAM Rev.* **17**, 274–297.

RILEY, N. & VASANTHA, R. 1989 Unsteady high Reynolds number flows. *J. Fluid Mech.* **205**, 243–262.

ROTT, N. 1956 Unsteady viscous flow in the vicinity of a stagnation point. *Q. Appl. Maths.* **13**, 444–451.

SEARS, W. R. & TELIONIS, D. P. 1971 Unsteady boundary-layer separation. In *Recent Research on Unsteady Boundary Layers*, pp. 404–447. Laval University Press, Quebec.

SEARS, W. R. & TELIONIS, D. P. 1975 Boundary-layer separation in unsteady flow. *SIAM J. Appl. Maths.* **28**, 215–235.

SMITH, F. T. 1982 Concerning dynamic stall, *Aeron. Q. Nov./Dec.*

SMITH, F. T. 1988 Finite-time breakup can occur in unsteady interacting boundary layer. *Mathematika* **35**, 256–273.

SMITH, C. R., WALKER, J. D. A., HAIDARI, A. H. & SOBRUN, U. 1991 On the dynamics of near-wall turbulence. *Phil. Trans. R. Soc. Lond.* A (in press).

SMITH, C. R., WALKER, J. D. A., HAIDARI, A. H. & TAYLOR, B. K. 1990 Hairpin vortices in turbulent boundary layers: the implications for reducing surface drag. In *2nd IUTAM Symp. on Structure of Turbulence and Drag Reduction.* (ed. A. Gyr). Springer.

VAN DOMMELEN, L. L. 1981 Unsteady boundary-layer separation, Ph.D dissertation, Cornell University.

VAN DOMMELEN, L. L. & COWLEY, S. J. 1990 On the Lagrangian description of unsteady boundary-layer separation. Part 1. General theory. *J. Fluid Mech.* **210**, 593–626.

VAN DOMMELEN, L. L. & SHEN, S. F. 1980 The spontaneous generation of the singularity in a separating boundary layer. *J. Comput. Phys.* **38**, 125–140.

VAN DOMMELEN, L. L. & SHEN, S. F. 1982 The genesis of separation. In *Proc. Symp. on Numerical and Physical Aspects of Aerodynamic Flow.* Long Beach, California, (ed. T.Cebeci), pp. 283–311. Springer.

WALKER, J. D. A. 1978 The boundary layer due to a rectilinear vortex. *Proc. R. Soc. Lond.* A **359**, 167–188.

WALKER, J. D. A. 1990*a* Wall-layer eruptions in turbulent flows, In *2nd IUTAM Sym. on Structure of Turbulence and Drag Reduction* (ed. A. Gyr). Springer; also *NASA Tech. Mem.* 102362, ICOMP-89-26.

WALKER, J. D. A. 1990*b* Models based on dynamical features of the wall layer, *Appl. Mech. Rev.* **43**, S232-S239.

WALKER, J. D. A., ABBOTT, D. E., SHARNHORST, R. K. & WEIGAND, G. G. 1989 Wall-layer model for velocity profile in turbulent flows. *AIAA J.* **27** , 140–149.

WALKER, J. D. A., SMITH, C. R., DOLIGALSKI, T. L. & CERRA, A. W. 1987 The impact of a vortex ring on a wall. *J. Fluid Mech.* **181**, 99–140.

WILLIAMS, J. C. 1977 Incompressible boundary-layer separation. *Ann. Rev. Fluid Mech.* **9** 113–144.